Plant Small RNA Species Direct Gene Silencing in Pathogenic Bacteria as well as Disease Protection

Meenu Singla-Rastogi[1], Magali Charvin[1§], Odon Thiébeauld[2§], Alvaro L Perez-Quintero[1], Antinéa Ravet[1], Antonio Emidio-Fortunato[2], Venugopal Mendu[1] & Lionel Navarro[1]*

[1] Institut de Biologie de l'Ecole Normale Supérieure (IBENS), 75005 Paris, France; Centre National de la Recherche Scientifique UMR8197, 75005 Paris France, Institut National de la Santé et de la Recherche Médicale U1024, 75005 Paris, France.

[2] ImmunRise, 46 Rue d'Ulm, 75005 Paris, France.

[§] These authors contributed equally to the work

*To whom correspondence should be addressed: lionel.navarro@ens.fr

Abstract

Plant small RNAs (sRNAs) and/or double-stranded RNAs (dsRNAs) trigger RNA interference (RNAi) in interacting eukaryotic pathogens or parasites. However, it is unknown whether this phenomenon could operate in bacterial phytopathogens, which lack a eukaryotic-like RNAi machinery. Here, we first show that Arabidopsis-encoded inverted repeat transgenes trigger silencing of *Pseudomonas syringae* heterologous reporter and endogenous virulence-associated genes during infection. Antibacterial Gene Silencing (AGS) of the latter was associated with a reduced pathogenesis, which was also observed upon application of corresponding plant-derived RNAs onto wild-type plants prior to infection. We additionally demonstrate that sRNAs directed against virulence factor transcripts were causal for silencing and pathogenesis reduction, while cognate long dsRNAs were inactive. Overall, this study provides the first evidence that plant sRNAs can directly reprogram gene expression in a phytopathogenic bacterium and may have wider implications in the understanding of how plants regulate transcriptome, community composition and genome evolution of associated bacteria.

Introduction

RNAi is a conserved gene regulatory mechanism that has been characterized as an antiviral defense response by repressing translation, accumulation and/or replication of viral RNAs[1]. In plants, RNAi has also been shown to control resistance against bacterial, fungal and oomycete pathogens partly by fine-tuning the expression of immune-responsive genes[2,3]. The core mechanism of RNAi involves the processing of dsRNAs or single-stranded RNAs (ssRNAs) carrying stem loop structures (e.g. primary microRNA –miRNA– transcripts) by DCL proteins leading to the production of 20-25 nt long short interfering RNAs (siRNAs) or miRNAs. siRNAs or miRNAs are then loaded into Argonaute (AGO) proteins to direct post-transcriptional silencing of sequence complementary mRNA targets through endonucleolytic

cleavage and/or translational inhibition[4].

An important feature of plant sRNAs, and particularly of siRNAs, is their ability to trigger non-cell autonomous silencing in adjacent cells as well as in distal tissues[5,6]. This phenomenon is essential to prime antiviral response ahead of the infection front but also to translocate silencing signals between plant cells and their non-viral eukaryotic interacting (micro)organisms[7,8]. For example, plant sRNAs were previously found to be exported in the fungal pathogens *Verticillium dahliae*[9] and *Botrytis cinerea*[10] as well as in the oomycete pathogen *Phytophthora capsici*[11], leading to the silencing of pathogenicity factors. On the other hand, fungal siRNAs from *B. cinerea* were shown to be translocated into plant cells to silence defense genes[12], highlighting bidirectional RNAi in a natural plant-fungal interaction. In addition, a very recent report provides evidence that rhizobial tRNA-derived sRNAs can silence legume symbiotic genes[13]**.** However, whether plant sRNAs can in turn directly reprogram gene expression in plant-associated bacteria remains unknown.

Artificial trans-kingdom RNAi has long been employed to direct Host-Induced Gene Silencing (HIGS), a technology used to characterize the function of fungal and oomycete genes or to engineer disease resistance in plants. HIGS notably relies on *in planta* expression of dsRNAs bearing homologies to essential and/or virulence genes and can operate in insects, nematodes, parasitic plants, oomycete and fungi. For example, HIGS confers full protection against *Fusarium graminearum*[14] and *B. cinerea*[10], a phenotype which can be recapitulated by spraying antifungal dsRNAs and/or siRNAs onto Arabidopsis wild type (WT) plants prior to infection[15,10]. The latter phenomenon is referred to as Spray-Induced Gene Silencing (SIGS) and is reminiscent of 'environmental RNAi', a process involving the uptake of RNAs from the environment to trigger RNAi[16,17]. However, so far, HIGS and SIGS have only been shown to be functional in eukaryotic (micro)organisms possessing canonical RNA silencing factors. Indeed, there is currently no evidence indicating that host-encoded dsRNAs and/or sRNAs

could direct gene silencing in interacting phytopathogenic bacteria, which lack conventional eukaryotic-like RNAi factors. It is also unknown whether external application of any of these RNA entities could trigger environmental RNAi in pathogenic prokaryotic cells and if such hypothetical RNA-based regulatory process could be used to protect plants towards bacterial diseases. Here, we wanted to test these intriguing ideas using *Pseudomonas syringae* pv. *tomato* strain DC3000 (*Pto* DC3000) as an experimental model system.

Results

Pto DC3000 is a Gram-negative bacterium that is the causal agent of bacterial speck disease in tomato and can also infect *Arabidopsis thaliana*[18]. This bacterium enters into leaf tissues through stomata or wounds and further multiplies in the apoplast[19]. To assess whether plant sRNAs and/or dsRNAs could reprogram *Pto* DC3000 gene expression, we first targeted a chromosomally integrated *Photorhabdus luminescens luxCDABE* reporter driven by the constitutive kanamycin promoter[20]. This *lux*-tagged *Pto* DC3000 (*Pto* WT LUC) strain spontaneously emits luminescence because it co-expresses the luciferase catalytic components *luxA* and *luxB* genes along with the genes required for substrate production, namely *luxC, luxD* and *luxE*[21] (Fig.1a). Two independent Arabidopsis transgenic lines that constitutively express a chimeric inverted repeat which carries sequence homology with the coding regions of *luxA* and *luxB* were selected on the basis of their ability to produce anti-*luxA* and anti-*luxB* siRNAs (Fig.1b). They were subsequently syringe-infiltrated with the *lux*-tagged *Pto* DC3000 strain and the levels of luminescence activity were monitored at 24 hours post-inoculation (hpi). A significant reduction in luminescence activity was found in IR-*LUXA/LUXB*-compared to control Col-0-infected plants (Fig.1c). By contrast, the growth of the bacterial reporter strain remained unchanged in the apoplast of IR-*LUXA/LUXB* lines compared to Col-0 plants (Fig.1d), indicating that the above effects were not due to a decreased bacterial titer

in these transgenic lines. Furthermore, a significant reduction in the accumulation of both *luxA* and *luxB* mRNAs was found in IR-*LUXA/LUXB*- compared to control Col-0-infected plants, while the levels of the non-targeted *proC* bacterial transcripts remained unchanged (Fig.1e). These data indicate that an Arabidopsis-encoded inverted repeat can trigger silencing of *Pto* DC3000 heterologous reporter genes during infection.

Pto DC3000 possesses a large repertoire of pathogenicity factors, among them the type III secretion system (TTSS) and the phytotoxin coronatine (COR), which mimics the most active isoleucine conjugate of the phytohormone Jasmonic Acid (JA), both being critical for pathogenesis[22-25]. To investigate whether Antibacterial Gene Silencing (AGS) could be additionally effective against endogenous *Pto* DC3000 genes that are relevant for pathogenesis, we next generated Arabidopsis transgenic plants that constitutively express a chimeric inverted repeat carrying sequence homology with the coding regions of the *coronafacic acid polyketide synthase I* (*cfa6*) gene and of the *hrpL* alternative sigma factor of *Pto* DC3000 (Fig.2a). The former bacterial factor is essential for the biosynthesis of coronafacic acid (CFA), which is a major structural component of COR[26], while the latter controls directly the expression of type III-secretion system associated genes and indirectly the expression of COR biosynthesis genes[27, 28]. As a negative control, we have generated Arabidopsis transgenic lines overexpressing an inverted repeat, which does not exhibit sequence homology with the *Pto* DC3000 genome, but instead targets three cytochrome P450 lanosterol C-14α-demethylase (*CYP51*) genes of the fungal pathogen *F. graminearum*[14]. These stable transgenic lines are referred to as IR-*CFA6/HRPL* and control vector (CV) plants, respectively, and do not exhibit any developmental defect compared to Col-0 plants, despite high accumulation of artificial siRNAs (Fig.2b, 2c; Supplementary Fig.2). Additional characterization of the reference IR-*CFA6/HRPL#4* transgenic line by sRNA sequencing, revealed high and comparable levels of anti-*cfa6* and anti-*hrpL* siRNAs, with a bias towards

21 nt siRNAs (Fig.2d). Furthermore, siRNAs were produced along the *CFA6* and *HRPL* regions of the chimeric inverted repeat (Fig.2e), which is consistent with a processive cleavage of the *CFA6/HRPL* dsRNA precursors by DCL proteins. An sRNA target prediction analysis against the *Arabidopsis thaliana* and *Pto* DC3000 annotated genes also indicated that an off-target effect seems unlikely (Supplementary Fig.1, Table S1, S2).

We further dip-inoculated these transgenic plants with *Pto* DC3000 and monitored *cfa6* and *hrpL* mRNA levels by RT-qPCR analyses at 3 days-post infection (dpi). While the *cfa6* mRNA levels were moderately altered in two out of three independent IR-*CFA6/HRPL* lines compared to Col-0 plants, the levels of *hrpL* transcripts were reproducibly and significantly reduced in all the three IR-*CFA6/HRPL* lines compared to Col-0 plants (Fig.2f). By contrast, the down-regulation of *cfa6* or *hrpL* mRNAs was not observed in CV- *versus* Col-0-infected plants (Fig.2f), supporting a specific effect of these antibacterial RNAs. In addition, the mRNA level of the non-targeted *proC* gene was unchanged in IR-*CFA6/HRPL*-infected lines compared to Col-0- or CV-infected plants (Fig.2f). We conclude that the Arabidopsis-encoded IR-*CFA6/HRPL* transgene can at least trigger silencing of the *Pto* DC3000 *hrpL* gene during infection.

It has been previously reported that *Pto* DC3000 triggers the reopening of stomata as a counter-defense towards plant-induced stomatal closure, which is rapidly orchestrated upon bacterial detection[29]. This virulence response is critical for *Pto* DC3000 pathogenesis as it allows bacterial cells to reach the apoplast and to colonize inner leaf tissues. Previous studies have also shown that COR plays a major role in *Pto* DC3000-induced stomatal reopening[30]. Accordingly, the COR-deficient *Pto* DC3118 strain, which is specifically mutated in the *cfa6* gene and referred to here as *Pto* DC3000 Δ*cfa6* (*Pto*Δ*cfa6*), is not able to reopen stomata at 3 hpi (Fig.3a, Supplementary Fig.3a). Similarly, we found that the *Pto* DC3000 Δ*hrpL* (*Pto*Δ*hrpL*) strain, which is also deficient in COR biosynthesis[24], was not capable of

reopening stomata (Fig.3a, Supplementary Fig.3a). On the contrary, and as shown previously[30], a normal stomatal reopening phenotype was observed during infection with the type III secretion-defective *Pto* DC3000*hrcC* mutant (*Pto*Δ*hrcC*) (Fig.3a; Supplementary Fig.3a), indicating that at this infection timepoint, type III effectors appear to be dispensable for this response.

We next monitored *Pto* DC3000-induced stomatal reopening response in IR-*CFA6/HRPL* transgenic lines. Significantly, these plants were fully insensitive to the stomatal reopening response typically triggered by *Pto* DC3000 at 3 hpi (Fig.3b; Supplementary Fig.3b), thereby mimicking the phenotypes observed during infection of Col-0 plants with the *Pto*Δ*cfa6* or the *Pto*Δ*hrpL* strains (Fig.3a, 3b; Supplementary Fig.3a, 3b). By contrast, *Pto* DC3000-triggered stomatal reopening events were unaltered in CV- compared to Col-0-infected plants (Fig.3c; Supplementary Fig.3c), supporting a specific effect of antibacterial RNAs in this process. In addition, the altered stomatal reopening phenotype detected in IR-*CFA6/HRPL* plants infected with the WT *Pto* DC3000 strain, and in Col-0 plants challenged with the *Pto*Δ*cfa6* or the *Pto*Δ*hrpL* strains, was fully rescued upon exogenous application of COR (Fig.3a, 3b; Supplementary Fig.3a, 3b). These data provide pharmacological evidence that the reduced *Pto* DC3000 pathogenesis manifested at infected IR-*CFA6/HRPL* stomata is likely caused by an altered ability of the associated and/or surrounding bacterial cells to produce COR.

We next assessed the impact that AGS could have on the ability of *Pto* DC3000 to colonize the apoplast of surface-inoculated leaves, a phenotype which is dependent on both type III effectors and COR[22]. To this end, we dip-inoculated Col-0, CV and IR-*CFA6/HRPL* plants with *Pto* DC3000 and subsequently monitored bacterial titer at 2 dpi. We found that *Pto* DC3000 was less effective in colonizing the apoplast of IR-*CFA6/HRPL* lines compared to Col-0 and CV-infected plants, a phenotype that was comparable to the growth defect of the *Pto*Δ*cfa6* strain in Col-0 plants (Fig.4a). Nevertheless, this phenotype was less pronounced

than the one observed with the *Pto*Δ*hrpL* strain grown on Col-0 plants (Supplementary Fig.4a), which might be due to the partial silencing of the targeted virulence factors and/or to the known RNA silencing suppression activity triggered by *Pto* DC3000 (Fig.2f)[31, 32]. In addition, we noticed that IR-*CFA6/HRPL* plants dip-inoculated with *Pto* DC3000 showed reduced water-soaking symptoms at 1 dpi (Fig.4b), thereby phenocopying Col-0 plants dip-inoculated with the *Pto*Δ*cfa6* or the *Pto*Δ*hrpL* strains (Supplementary Fig.4b). Therefore, AGS can alter the ability of *Pto* DC3000 to trigger water-soaking and to multiply in the apoplast of Arabidopsis leaves, which are both critical steps of bacterial pathogenesis[33].

Next, we assessed whether AGS could interfere with the capacity of *Pto* DC3000 to colonize xylem vessels, which is the main route used by this bacterium to propagate in the leaf vasculature[34, 35]. This *Pto* DC3000 virulence phenotype has been recently characterized and found here to be dependent on both type III effectors and COR (Supplementary Fig.4c, 4d). For this purpose, we wound-inoculated the leaf midvein of IR-*CFA6/HRPL* plants with a *GFP*-tagged *Pto* DC3000 (*Pto* DC3000-GFP) and further scored the number of bacterial propagation from inoculation sites. We found a strong decrease in *Pto* DC3000-GFP vascular propagation in the IR-*CFA6/HRPL* lines compared to Col-0- and CV-infected plants (Fig.4c, 4d), thereby mimicking the impaired spreading phenotype of the *Pto*Δ*cfa6*-GFP and *Pto*Δ*hrpL*-GFP strains on Col-0 plants (Supplementary Fig.4c). Altogether, these data demonstrate that AGS can limit pathogenesis of *Pto* DC3000 in different tissues of Arabidopsis transgenic plants.

Environmental RNAi is a phenomenon by which (micro)organisms uptake external RNAs from the environment, resulting in the silencing of genes containing sequence homologies to the RNA triggers[17]. This process has been initially characterized in *Caenorhabditis elegans*[36-39] and was further found to operate in other nematodes but also in insects, plants and fungi[15,40]. However, this approach has never been used against a bacterial phytopathogen that

lacks a canonical eukaryotic-like RNAi machinery such as *Pto* DC3000. To test this possibility, we first assessed whether RNA extracts from IR-*CFA6/HRPL* plants could trigger silencing of *cfa6* and *hrpL* genes in *in vitro* conditions. For this purpose, we incubated total RNAs from CV and IR-*CFA6/HRPL* plants with *Pto* DC3000 cells, and further analyzed by RT-qPCR the levels of *cfa6* and *hrpL* mRNAs. Results from these analyses revealed a reduction in the accumulation of both virulence factor mRNAs upon treatment with RNA extracts from IR-*CFA6/HRPL* plants (Fig.5a). By contrast, the level of the non-targeted *proC* and *rpoB* mRNAs remained unaltered in the same conditions (Fig.5a). These data imply that plant antibacterial RNAs are likely taken-up by *Pto* DC3000 cells and subsequently trigger gene silencing in these prokaryotic cells. It also suggests that exogenous application of these antibacterial RNAs could be used as a strategy to dampen pathogenesis. To test this idea, we pre-treated Arabidopsis Col-0 leaf sections with total RNAs from IR-*CFA6/HRPL* plants for one hour, subsequently challenged them with *Pto* DC3000, and further monitored stomatal reopening events at 3 hpi. Strikingly, we found that RNA extracts from IR-*CFA6/HRPL* plants fully suppressed the ability of *Pto* DC3000 to reopen stomata (Fig.5b; Supplementary Fig.6a), thereby mimicking the phenotype observed in infected IR-*CFA6/HRPL* leaves (Fig.3b; Supplementary Fig.3b). We additionally investigated whether this approach could be used to control the growth of *Pto* DC3000 *in planta*. For this purpose, we pre-treated for one hour Arabidopsis Col-0 plants with total RNAs from IR-*CFA6/HRPL* plants and further dip-inoculated them with *Pto* DC3000. We found that these RNA extracts triggered a decreased *Pto* DC3000 titer at 2 dpi, a phenotype that was comparable to the ones observed in IR-*CFA6/HRPL* and Col-0 plants inoculated with the *Pto*Δ*cfa6* strain (Fig.4a, 5c). By contrast, application of total RNAs from CV plants did not alter growth of *Pto* DC3000 in the same conditions (Fig.5c), supporting a specific effect of antibacterial RNAs in this process. To assess whether such RNA-based biocontrol approach could also be effective in cultivated

plants, we repeated the same assay on tomato (*Solanum lycopersicum*), which is the natural host of *Pto* DC3000. Pre-treatment of WT tomato leaves for one hour with RNA extracts from IR-*CFA6/HRPL* plants led to compromised *Pto* DC3000-induced necrotic disease symptoms and to a reduction in bacterial content compared to leaves pre-treated with RNA extracts from CV plants (Fig.5d, 5e, 5f; Supplementary Fig.5a, 5b, 5c). Collectively, these data demonstrate that external application of plant antibacterial RNAs can trigger AGS and disease protection against *Pto* DC3000 in both Arabidopsis and tomato plants.

Next, we interrogated which RNA entities are responsible for AGS upon external application of antibacterial RNAs. We first introduced the *dcl2-1, dcl3-1* and *dcl4-2* mutations in the IR-*CFA6/HRPL#4* reference line. These resulting IR-*CFA6/HRPL#4 dcl234* plants revealed high accumulation of IR-*CFA6/HRPL* transcripts, despite probable transcriptional repression of the $35S_{pro}$:IR-*CFA6/HRPL* transgene due to the use of T-DNA insertional mutant carrying the 35S promoter (Fig.6a)[41, 42]. Furthermore, anti-*cfa6* and anti-*hrpL* siRNAs were undetectable in those plants (Fig.6b), which is consistent with a role of DCL2, DCL3 and DCL4 in the processing of IR-*CFA6/HRPL*. We subsequently extracted total RNAs from these plants, incubated them with *Pto* DC3000 cells, and further monitored *cfa6* and *hrpL* mRNA levels by RT-qPCR analysis. Using this *in vitro* assay, we found that RNA extracts from IR-*CFA6/HRPL#4 dcl234* plants were no longer able to trigger down-regulation of *cfa6* and *hrpL* mRNAs (Fig.6c), despite high accumulation of *CFA6/HRPL* dsRNA precursor transcript (Fig.6a). By contrast, RNA extracts from the IR-*CFA6/HRPL#4* plants, which contain high levels of anti-*cfa6* and anti-*hrpL* siRNAs (Fig.2c, 6b), triggered reduced accumulation of these bacterial mRNAs (Fig.5a, 6c).

We next decided to analyze the antibacterial activity of the above RNA extracts by monitoring their effects on stomatal reopening of Col-0-infected plants. A prerequisite for this assay was to verify that Col-0 leaf sections would not trigger the processing of *CFA6/HRPL*

dsRNAs, and thus the production of anti-*cfa6* and anti-*hrpL* siRNAs, upon incubation with RNA extracts from IR-*CFA6/HRPL#4 dcl234* plants, which was validated by northern blot analysis (Fig.6d, Supplementary Fig.6b). Interestingly, when we further monitored stomatal aperture in Col-0-infected leaf tissues pre-treated for one hour with these RNA entities, we found that *Pto* DC3000 triggered normal stomata reopening, thereby mimicking the effect observed with control RNAs from Col-0 or *dcl234* plants (Fig.6e; Supplementary Fig.6c). By contrast, RNA extracts from IR-*CFA6/HRPL#4* plants, which contain abundant anti-*cfa6* and anti-*hrpL* siRNAs, triggered full suppression of stomatal reopening in the same conditions (Fig.6d, 6e). Collectively, these data indicate that *CFA6/HRPL* long dsRNAs are neither involved in AGS nor in pathogenesis reduction. They rather suggest that corresponding siRNAs are likely the RNA entities responsible for these phenotypes. To verify this assumption, we further purified sRNA species from IR-*CFA6/HRPL* plant total RNAs using a glass fiber filter-based method (Supplementary Fig.7a, 7b), and subjected them to stomatal reopening assay. We found that these sRNA species suppressed *Pto* DC3000-triggered stomatal reopening, to the same extent as IR-*CFA6/HRPL* plant total RNA extracts (Fig.6f; Supplementary Fig.7c). By contrast, long RNA species, which were not filtered through the above columns, were inactive (Fig.6f; Supplementary Fig.7c), further supporting that *CFA6/HRPL* long dsRNAs are not involved in this response. We have then synthesized *CFA6/HRPL* long dsRNAs and cognate double-stranded siRNAs *in vitro* to further test their antibacterial activity (Fig.6g). The *in vitro*-synthesized *CFA6/HRPL* long dsRNAs did not alter the ability of *Pto* DC3000 to reopen stomata, nor did *CYP51* long dsRNAs used as controls (Fig.6h; Supplementary Fig.7d). By contrast, *in vitro*-synthesized anti-*cfa6* and anti-*hrpL* siRNAs fully suppressed stomatal reopening (Fig.6h; Supplementary Fig.7d), and accordingly, triggered silencing of *cfa6* and *hrpL* genes (Fig.6i). Altogether, these data

provide evidence that siRNAs directed against *cfa6* and *hrpL* genes are critical for AGS and pathogenesis reduction, while cognate long dsRNAs are ineffective for both processes.

Although the above findings indicate that siRNAs can trigger AGS and antibacterial activity, they do not firmly demonstrate that these RNA entities are causal for these phenomena. To address this, we decided to generate recombinant bacteria expressing a siRNA-resilient version of the *hrpL* gene. To this end, we complemented the *Pto*Δ*hrpL* mutant with either a WT *hrpL* transgene or a mutated version that contains as many silent mutations as possible in the siRNA targeted region, which were predicted to alter the binding of siRNAs with the *hrpL* mRNA but to produce the same protein sequence (Fig.7a, 7b, Supplementary Table3). Both transgenes were expressed under the constitutive neomycin phosphotransferase II (*NPTII*) promoter (Fig.7c). The resulting recombinant bacteria, referred to as *Pto*Δ*hrpL* WT *hrpL* and *Pto*Δ*hrpL* mut *hrpL*, were found to restore the ability of the *Pto*Δ*hrpL* strain to reopen stomata when inoculated on Col-0 leaf sections (Fig.7f; Supplementary Fig.9a, 9b), indicating that both transgenes are functional in a stomatal reopening assay. We further assessed the sensitivity of each recombinant bacterium to AGS. For this purpose, we incubated *Pto*Δ*hrpL* WT *hrpL* and *Pto*Δ*hrpL* mut *hrpL* strains with total RNA extracts from CV and IR-*CFA6/HRPL#4* plants and further monitored *hrpL* transgene mRNA levels by RT-qPCR analysis. We found a significant decrease in the accumulation of *hrpL* mRNAs expressed from the *Pto*Δ*hrpL* WT *hrpL* strain, which was not detected upon treatment with RNA extracts from CV plants (Fig.7d). These data indicate that the WT *hrpL* transgene expressed from the *Pto*Δ*hrpL* WT *hrpL* strain is sensitive to AGS despite its constitutive expression driven by the *NPTII* promoter. By contrast, the accumulation of *hrpL* mRNAs expressed from the *Pto*Δ*hrpL* mut *hrpL* strain was unaltered in response to RNA extracts from IR-*CFA6/HRPL#4* plants (Fig.7d), indicating that siRNAs no longer exert their AGS effect

towards this recombinant bacterium. Collectively, these findings demonstrate that anti-*hrpL* siRNAs are causal for silencing of the *hrpL* gene in *Pto* DC3000 cells.

We finally investigated the responsiveness of each recombinant bacterial strain to siRNA-directed pathogenesis reduction by exploiting the *Pto* DC3000-induced stomatal reopening assay. To assess the specific effect of siRNAs towards suppression of *hrpL*-mediated stomatal reopening function, we cloned an IR-*HRPL* inverted repeat targeting the same *hrpL* sequence region than the one targeted by the IR-*CFA6/HRPL* hairpin, and further validated its capacity to produce anti-*hrpL* siRNAs upon Agrobacterium-mediated transient expression in *Nicotiana benthamiana* leaves (Fig.7e). *N. benthamiana* total RNAs containing anti-*hrpL* siRNAs were found to fully suppress the ability of *Pto* DC3000 to reopen stomata (Fig.7f, Supplementary Fig.8). Importantly, similar results were obtained when *N. benthamiana* RNA extracts containing anti-*hrpL* siRNAs were incubated with the *Pto*Δ*hrpL* WT *hrpL* strain (Fig.7f; Supplementary Fig.9a, 9b), supporting a sensitivity of this bacterial strain to siRNA action. By contrast, the *Pto*Δ*hrpL* mut *hrpL* strain was fully competent in reopening stomata (Fig.7f; Supplementary Fig.9a, 9b), indicating that anti-*hrpL* siRNAs no longer exert their antibacterial effects towards this recombinant bacterium. Similar results were also observed in Arabidopsis stable IR-*HRPL* transgenic lines overexpressing anti-*hrpL* siRNAs (Fig.7g, 7h; Supplementary Fig.9c). This indicates that the suppression of stomatal reopening phenotype is not due to potential off-target effects of these host-encoded siRNAs but rather caused by their targeting effects over the *hrpL* transcript sequence. Altogether, these data provide sound evidence that anti-*hrpL* siRNAs are causal for the suppression of *hrpL*-mediated stomatal reopening function. They also further validate a novel role of *hrpL* in bacterial-induced stomatal reopening, indicating that AGS can be employed as a tool to characterize bacterial gene function.

Discussion

We show here that Arabidopsis-encoded siRNAs trigger the silencing of *Pto* DC3000 virulence-associated genes, resulting in the dampening of pathogenesis. In particular, we found that anti-*cfa6* and/or anti-*hrpL* siRNAs fully suppressed *Pto* DC3000-induced stomatal reopening, a virulence response that is dependent on the production of COR by epiphytic bacterial cells[46]. Our data therefore indicate that antibacterial siRNAs can act at the pre-invasive stage of the infection, presumably by preventing COR biosynthesis in *Pto* DC3000 cells that come in contact with the leaf surface. In addition, we found that AGS was capable of reducing the ability of *Pto* DC3000 to mount water-soaking symptoms, to multiply in the leaf apoplast and to propagate in the leaf vasculature of Arabidopsis. Therefore, siRNAs additionally act at a post-invasive stage of the infection by targeting endophytic bacterial cells present in the apoplast and in xylem vessels. These observations imply that siRNAs must be externalized from plant cells towards the leaf surface, the apoplast and xylem vessels in order to reach epiphytic and endophytic bacterial populations. One siRNA trafficking mechanism might involve plant extracellular vesicles (EVs), whose secretion is enhanced during antibacterial defense and which contain diverse species of sRNAs[43, 44]. Such a hypothesis would be consistent with recent findings showing that EVs ensure the movement of siRNAs from plant cells to fungal or oomycete cells[7,11]. It would also be congruent with a recent report showing that plant-derived exosome-like nanoparticles ingested by mice deliver plant miRNAs into specific commensal bacteria to reprogram their gene expression[45]. In accordance with these studies, we found that EVs isolated from the Arabidopsis IR-*CFA6/HRPL#4* leaf apoplast, which were in a size range between 50 to 300 nm[44] (Fig.8a; Supplementary Fig.10a), were fully competent in suppressing stomatal reopening, as observed with the apoplastic fluid from these transgenic plants (Fig.8b; Supplementary Fig.10b, 10d,

10f). This suggests that apoplastic EVs may, at least in part, contribute to the trafficking of sRNAs from plant cells towards *Pto* DC3000 cells.

We additionally showed that incubating RNA extracts containing antibacterial siRNAs with *Pto* DC3000 cells was sufficient to trigger AGS. However, corresponding dsRNAs were ineffective for this process, suggesting that the latter RNA entities are either not taken-up by, or not properly processed in, *Pto* DC3000 cells. This is a major distinction from environmental RNAi in *C. elegans* and plant herbivores, which specifically relies on long dsRNAs[37-40,46], or in filamentous pathogens, which is triggered by both dsRNAs and siRNAs[15,10]. Instead, we found that plant siRNA species were causal for environmental RNAi in *Pto* DC3000, and this regulatory process was even, intriguingly, recapitulated in the presence of *in vitro*-synthesized siRNA duplexes. These data imply that *Pto* DC3000 must additionally be capable of taking-up –passively and/or actively– free sRNAs, despite the presence of a cell wall and an intricate double membrane structure. The data also suggest that *Pto* DC3000 must have evolved a machinery to take charge of the internalized sRNAs and direct gene silencing in bacterial cells. It will thus be appealing to identify such prokaryotic factors and to elucidate the principles of sRNA target recognition and mode of action in bacterial cells. Investigating whether our findings also apply to endogenous plant sRNAs, and assessing their possible implications in the regulation of the transcriptome, community composition and genome evolution of plant-associated bacteria will represent exciting directions for future studies.

Material and Methods

Plasmid construction

The IR-*CFA6/HRPL* construct is composed of 250 bp regions of *Pto* DC3000 genes, *cfa6* (1-250 nt) and *hrpl* (99-348 nt), aligned in sense and antisense directions with the intron of the petunia chalcone synthase gene (*CHSA)* in between. The control vector (CV) construct IR-*CYP51* is composed of described conserved regions from *F. graminearum CYP51A*, *CYP51B* and *CYP51C*[13] and the IR-*LUXA/LUXB* is composed regions from *luxA* and *luxB* genes of the *luxCDABE* operon and they are aligned in sense and antisense directions with the same intron sequence as described above. The IR-*CFA6/HRPL*, IR-*CYP51* and IR-*LUXA/LUXB* constructs containing *EcoRI* and *SalI* sites at both extremities were synthesized by GenScript® and inserted by restriction enzymatic digestion into a modified pDON221-P5-P2 vector carrying additional *EcoRI* and *SalI* sites to facilitate the insertion of these long-inverted repeats. The plasmids containing the $35S_{pro}$:IR-*CFA6*/*HRPL* and $35S_{pro}$:IR-*CYP51* were obtained by a double recombination between pDON221-P5-P2 carrying the inverted repeat sequences and pDON221-P1-P5r carrying the Cauliflower Mosaic Virus (CaMV) 35S promoter sequence, in the the pB7WG Gateway destination vector using LR clonase plus (Life Technologies). These plasmids were then introduced into the Agrobacterium C58C1 strain. The IR-*HRPL* construct, which is composed of the same 250 bp region of *hrpL* as in the IR-*CFA6/HRPL* construct, was recombined by using GreenGate technology[47] to constitute the plasmid $35S_{pro}$:IR-*HRPL*, which was then transformed in the Agrobacterium C58C1 strain. To generate the WT *hrpL* and the mut *hrpL* plasmids, the wild type *hrpL* sequence was amplified from the genomic DNA isolated from *Pto* DC3000, while the mutant *hrpL* sequence was amplified from a mutated sequence synthesized by GenScript®. These two sequences were further cloned into pDON207 vector using BP clonase (Life Technologies) and then introduced by recombination using LR clonase (Life Technologies) into the pBS0046 destination vector, which carries a

constitutive NPTII promoter. Specific primers used for the purpose of cloning are listed in Supplementary table 4.

Plant material and growth conditions

Stable transgenic lines expressing IR-*LUXA/LUXB*, IR-*CFA6/HRPL*, IR-*CYP51* (CV) and IR-*HRPL* constructs were generated by transforming Arabidopsis (accession Col-0) plants using Agrobacterium mediated-floral dip method[48]. Two independent Arabidopsis T2 transgenic lines of IR-*LUXA/LUXB*, *#18* and *#20*; three independent Arabidopsis T4 transgenic lines of IR-*CFA6/HRPL*, *#4*, *#5* and *#10*; two independent Arabidopsis T2 transgenic lines of IR-*HRPL*, *#1* and *#4* and one reference Arabidopsis T4 transgenic line for IR-*CYP51 #2* (CV) were generated and used in our experiments. For genetic analysis, *dcl2-1 dcl3-1 dcl4-2* (*dcl234*) triple mutant was crossed with the reference line IR-*CFA6/HRPL#4* and the F3 plants were genotyped to select homozygous *dcl234* mutant containing the IR-*CFA6/HRPL* transgene. Sterilized seeds of Arabidopsis Col-0 and the selected homozygous transgenic lines were first grown for 12-14 days at 22°C on plates containing ½ x MS medium (Duchefa), 1% sucrose and 0.8 % agar (with or without antibiotic selection) in 8h photoperiod. Seedlings were then pricked out to soil pots and grown in environmentally controlled conditions at 22°C/ 19°C (day/night) with an 8h photoperiod under light intensity of 100 $\mu E/m^2/s$. Four- to five-week-old plants were used for all the experiments. Seeds of tomato (*Solanum lycopersicum* 'Moneymaker') and *Nicotiana benthamiana* were directly germinated on soil pots and grown in environmentally controlled conditions at 22 °C/ 19°C (day/night) with a 16h photoperiod under light intensity of 100 $\mu E/m^2/s$. Four- to five-week old plants were used for all the experiments.

Bacterial strains

The *PtoΔcfa6*-GFP (*Pto* DC3118-GFP) strain is a gift from S. Y. He, while the *PtoΔhrpL* strain is a gift from C. Ramos[49]. The *PtoΔhrpL* strain expressing the *GFP* reporter gene was generated by transformation with the GFP-pPNpt Green plasmid by electroporation and then plated on NYGB medium (5 g L^{-1} bactopeptone, 3 g L^{-1} yeast extract, 20 ml L^{-1} glycerol) containing gentamycin (1 µg mL^{-1}) for selection at 28 °C. To generate the *Pto* DC3000 WT *hrpL* and mut *hrpL* strains, the *PtoΔhrpL* strain was transformed with the plasmids $NPTII_{pro}$:WT-*hrpL* and $NPTII_{pro}$:mut-*hrpL*, respectively, by electroporation and then plated in NYGB medium with gentamycin (1 µg mL^{-1}) at 28°C for two days. The colonies containing the plasmid were selected by PCR using specific primers to *hrpL* gene. The lux-tagged *Pto* DC3000 strain has been previously described[21].

Bacterial infection assays in plants

(a) Bacterial dipping assay: Three hours after the beginning of the night cycle in growth chamber, three plants per condition were dip-inoculated with *Pto* DC3000 at 5 x 10^7 cfu ml^{-1} supplemented with 0.02 % Silwet L-77 (Lehle seeds). Plants were then immediately placed in chambers with high humidity. Water-soaking symptoms were observed 24 hours post-infection and pictures of representative leaves were taken. Two days post-inoculation, bacterial titer was measured for individual infected leaves (n=8). To quantify bacterial transcripts in infected plants, pool of infected leaves from three plants was collected three days post-inoculation.

(b) Wound-inoculation assay: Bacterial propagation in the mid-veins was assessed as described previously[34]. Around 15 leaves from three plants per condition were inoculated with a toothpick dipped in *GFP*-tagged bacteria at a concentration of 5 x 10^6 cfu ml^{-1} and then the plants were covered for 3 days. Bacterial propagation was then analyzed by monitoring GFP

signal under a UV light using an Olympus MV 10 × Macrozoom with a GFP filter and representative pictures of bacterial propagation were taken with a CCD camera AxioCam Mrc Zeiss.

(c) Plant protection assay: Prior to bacterial infection, four leaves of three Col-0 plants were dipped with mock solution (water) or 20 ng μl^{-1} of specific total RNAs, both supplemented with 0.02% of Silwet L-77. After one hour, leaves were dip-inoculated with *Pto* DC3000 WT or *PtoΔcfa6* at 5 x 10^7 cfu ml^{-1} with 0.02% of Silwet L-77. Bacterial titers were monitored two days post-inoculation, as specified earlier. Similar assay was performed using tomato plants but with a *GFP*-tagged *Pto* DC3000. Representative pictures of bacterial disease symptoms observed at 3 dpi were depicted.

(d) Bacterial luminescence quantification: Three plants per condition were syringe-infiltrated with the *lux*-tagged *Pto* DC3000 strain at 10^6 cfu ml^{-1}. Plants were placed in a chamber with high humidity to facilitate proper infection. After 24 hours, leaf discs were prepared and placed in individual wells of a 96 well plate to quantify the luminescence using Berthold Centro LB 960 Microplate Luminometer. Four leaves per plant were taken into consideration. Leaf discs from individual leaves were collected and pooled to monitor bacterial titers as described in (a).

Tomato infection quantification

(a) GFP loci quantification: Tomato leaves infected with *Pto* DC3000-GFP strain were analyzed under a UV light using an Olympus MV 10x Macrozoom with a GFP filter and pictures were taken with a CCD camera AxioCam Mrc Zeiss. Number of GFP loci was quantified with ImageJ software for at least 10 pictures per condition. Individual leaves were collected to extract genomic DNA.

(b) Bacterial genomic DNA quantification: To quantify bacterial infection in the infected tomato plants, the amount of bacterial genomic DNA (gDNA) was measured relative to plant gDNA[50]. Genomic DNA was isolated from tomato leaf samples infected with *Pto* DC3000-GFP using the DNeasy plant mini kit (QIAGEN, Germany) according to the manufacturer's instructions. Using 1 ng of gDNA, qPCR was performed using Takyon SYBR Green Supermix (Eurogentec®) and GFP-specific primers. Amount of bacterial gDNA was normalized to that of tomato using *Ubiquitin*-specific primers. Primer sequences are listed in Supplementary table 4.

Agrobacterium-mediated transient expression of inverted repeats in *N. benthamiana*

To express the IR-*HRPL* hairpin and the IR-*CFA6/HRPL* chimeric hairpin transiently, the *A. tumefaciens* C58C1 strains carrying these plasmids were grown overnight in LB medium at 28°C. Cells were resuspended in a solution containing 10 mM MES, pH 5.6, 10 mM $MgCl_2$ and 200 µM acetosyringone at a final concentration of 0.5 OD_{600}. Cultures were incubated in the dark at room temperature for 5-6 hours before Agrobacterium-mediated infiltration in 4-week old *N. benthamiana*. After 3 days, leaves were harvested for total RNA extraction and molecular analyses.

Stomatal aperture measurements

Using intact leaves from three plants, sections were dissected and immersed in mock solution (water) or bacterial suspension at 10^8 cfu ml^{-1}. After 3 hours, unpeeled leaf sections were stained with 10 µg ml^{-1} propidium iodide (Sigma) and abaxial surface was observed under SP5 laser scanning confocal microscope. The stomatal aperture (width relative to length) was measured using ImageJ software for at least 50-70 stomata per condition. For RNA and vesicle treatments, the leaf sections were incubated with total RNAs or APF and P40 fraction

extracted from specified genotypes for one hour before incubation with the bacteria. In specified experiments, 1 µM of Coronatine (COR; Sigma) was supplemented to the bacterial suspension.

***In vitro* AGS assay**

To assess whether the transcripts of *Pto* DC3000 *cfa6* and *hrpL* can be directly targeted by the dsRNA and/or the siRNAs generated by the hairpin IR-*CFA6/HRPL*, 2 ml cultures of *Pto* DC3000 WT, *PtoΔhrpL* WT *hrpL* and *PtoΔhrpL* mut *hrpL* at 10^7 cfu ml^{-1} were treated for 4 and/or 8 hours, with 20 ng μl^{-1} of specified total RNA extracted from CV or IR-*CFA6/HRPL#4* transgenic plants. For each condition, bacteria were harvested and processed for molecular analyses.

Quantitative RT-PCR Analyses

To monitor plant-encoded transcripts, total RNA was extracted from plant samples using Nucleospin RNA plant kit (Macherey Nagel). 0.5 µg of DNase-treated RNA was reverse transcribed using qScript cDNA Supermix (Quanta Biosciences®). cDNA was then amplified by real time PCR reactions using Takyon SYBR Green Supermix (Eurogentec®) and gene-specific primers. Expression was normalized to that of Arabidopsis *Ubiquitin*. To monitor bacterial transcripts, total RNA was extracted from bacteria-infected plant samples or from *in vitro* treated bacteria using Nucleospin RNA kit. After DNAse treatment, 250 ng of total RNA was reverse transcribed using random hexamer primers and qScript Flex cDNA kit (Quanta Biosciences®) and then amplified by real time PCR reaction using gene-specific primers. Expression was normalized to that of *gyrA*. Real time PCR was performed in 384-well optical reaction plates heated at 95°C for 10 min, followed by 45 cycles of denaturation at 95°C for 15s, annealing at 60°C for 20s, and elongation at 72°C for 40s. A melting curve was

performed at the end of the amplification by steps of 1°C (from 95°C to 50°C). Primer sequences are listed in Supplementary table 3.

RNA Gel Blot Analyses

Accumulation of low molecular weight RNAs was assessed by Northern blot analysis as previously described[31]. Total RNA was extracted using TriZOL reagent and stabilized in 50% formamide and 30 µg of total RNAs were used. To generate specific ^{32}P-radiolabelled probes, regions of 150 bp to 300 bp were amplified from the plasmids using gene specific primers (Supplementary Table 4) and the amplicons were labeled by random priming (Prime-a-Gene® Labeling System, Promega). U6 was monitored as an equal loading control.

Separation of long and small RNA fractions

From 100 µg of TriZOL-extracted total RNA, long and small RNA fractions were separated using the mirVana miRNA isolation kit (Ambion®) according to the manufacturer's instructions. The long and small RNA fractions were visualized using agarose gel electrophoresis and further analyzed using Bioanalyzer 2100 (Agilent Technologies).

***In vitro* synthesis of Inverted Repeat (IR) RNAs**

In vitro synthesized RNAs were generated following the instruction of the MEGAscript® RNAi Kit (Life Technologies, Carlsbad, CA). Templates were amplified by PCR using gene specific primers containing the T7 promoter. PCR amplification was done in two steps with two different annealing temperatures to increase the specificity of primers annealing. After the amplification step, PCR products were purified by gel extraction using the PCR Clean-up kit (Macherey-Nagel) to eliminate any unspecific PCR products. To produce dsRNAs, the purified PCR products were used as templates for *in vitro* transcription performed according

to the MEGAscript RNAi Kit instructions (Life Technologies). After purification with the filter catridges, the corresponding dsRNAs were processed in 18-25 nt siRNAs by ShortCut® RNase III (NEB, Ipswich, MA) for 40 min at 37°C. siRNAs were then specifically purified by using the mirVana™ miRNA Isolation Kit (Life Technologies, Carlsbad, CA). Each step of this process was followed by gel electrophoresis (TAE 1X, 1% agarose gel for DNA amplification and 2% agarose gel for RNAs) to verify the quality of RNAs.

Apoplastic Fluid (APF) and Extracellular Vesicles (EVs) extraction

Extraction was done as previously described[17]. Briefly, sixty leaves of 5 week-old CV or IR-*CFA6/HRPL* plants were syringe-infiltrated with vesicle isolation buffer (20 mM MES, 2 mM CaCl2, 0.01 M NaCl, pH 6.0). Leaves were then placed inside a 20 ml needleless syringe that was inserted in a 50 ml Falcon and centrifuged at 900 g for 15 minutes at 4°C. The apoplastic fluid (APF) was collected and, to get rid of any cell debris, filtered through 0.45 µm filter before to be centrifuged at 10,000 g for 30 minutes at 4°C. The APF was subjected to an ultracentrifugation step at 40,000 g for 60 min at 4°C to pellet EV fraction (P40) that was washed with vesicle isolation buffer and pelleted again. The pellet was further resuspended in 2 ml of 20 µM Tris buffer pH=7.5 and stored at 4°C. The size and concentration of EVs from both the APF and P40 fractions were analyzed using a LM10 Nanoparticle Tracking Analysis device (Malvern)[51].

Bioinformatic analysis

Small RNA libraries were constructed and sequenced from four- to five-week old leaves of IR-*CFA6/HRPL#4*. Raw reads have been deposited at the NCBI SRA under Bioproject (PRJNA587213). Libraries were mapped against the *Arabidopsis thaliana* genome (v TAIR10.1 GCF_000001735.4) and the IR-*CFA6/HRPL* sequence using ShortStack (default

parameters)[52]. Coverage of mapped loci was obtained with the Genomic Alignments package in R[53]. Unique reads mapping to *cfa6* and *hrpL* in both replicates were extracted and quantified from ShortStack mapping results using samtools[54]. Each unique read was aligned against annotated Arabidopsis and *Pto* DC3000 coding sequences (CDS) using BLAST[55] (-e-value 10, -word_size 4, -ungapped, -reward 1, -penalty -1), and the top target (with lowest e-value) was kept for each read in each target set. Binding free energy was calculated for each read/target pair using RNAup (-interaction pairwise)[56].

References

1. Baulcombe, D.C. VIGS, HIGS and FIGS: small RNA silencing in the interactions of viruses or filamentous organisms with their plant hosts. *Curr Opin Plant Biol* **26**, 141-6 (2015).

2. Pumplin, N. & Voinnet, O. RNA silencing suppression by plant pathogens: defence, counter-defence and counter-counter-defence. *Nat Rev Microbio*l **11**, 745-60 (2013).

3. Staiger, D., Korneli, C., Lummer, M. & Navarro, L. Emerging role for RNA-based regulation in plant immunity. *New Phytol* **197**, 394-404 (2013).

4. Bologna, N.G. & Voinnet, O. The diversity, biogenesis, and activities of endogenous silencing small RNAs in Arabidopsis. *Annu Rev Plant Biol* **65**, 473-503 (2014).

5. Liu, L. & Chen, X. Intercellular and systemic trafficking of RNAs in plants. *Nat Plants* **4**, 869-878 (2018).

6. Melnyk, C.W., Molnar, A. & Baulcombe, D.C. Intercellular and systemic movement of RNA silencing signals. *EMBO J* **30**, 3553-63 (2011).

7. Cai, Q. et al. Plants send small RNAs in extracellular vesicles to fungal pathogen to silence virulence genes. *Science* **360**, 1126-1129 (2018).

8. Guo, Z., Li, Y. & Ding, S.W. Small RNA-based antimicrobial immunity. *Nat Rev Immunol* **19**, 31-44 (2019).

9. Zhang, T. et al. Cotton plants export microRNAs to inhibit virulence gene expression in a fungal pathogen. *Nat Plants* **2**, 16153 (2016).

10. Wang, M. et al. Bidirectional cross-kingdom RNAi and fungal uptake of external RNAs confer plant protection. *Nat Plants* **2**, 16151 (2016).

11. Hou, Y. et al. A Phytophthora Effector Suppresses Trans-Kingdom RNAi to Promote Disease Susceptibility. *Cell Host Microbe* **25**, 153-165 e5 (2019).

12. Weiberg, A. et al. Fungal small RNAs suppress plant immunity by hijacking host RNA interference pathways. *Science* **342**, 118-23 (2013).

13. Ren, B., Wang, X., Duan, J. & Ma, J. Rhizobial tRNA-derived small RNAs are signal molecules regulating plant nodulation. *Science* **365**, 919-922 (2019).

14. Koch, A. et al. Host-induced gene silencing of cytochrome P450 lanosterol C14alpha-demethylase-encoding genes confers strong resistance to Fusarium species. *Proc Natl Acad Sci U S A* **110**, 19324-9 (2013).

15. Koch, A. et al. An RNAi-Based Control of *Fusarium graminearum* Infections Through Spraying of Long dsRNAs Involves a Plant Passage and Is Controlled by the Fungal Silencing Machinery. *PLoS Pathog* **12**, e1005901 (2016).

16. Wang, M. & Jin, H. Spray-Induced Gene Silencing: a Powerful Innovative Strategy for Crop Protection. *Trends Microbiol* **25**, 4-6 (2017).

17. Wang, M., Thomas, N. & Jin, H. Cross-kingdom RNA trafficking and environmental RNAi for powerful innovative pre- and post-harvest plant protection. *Curr Opin Plant Biol* **38**, 133-141 (2017).

18. Mansfield, J. et al. Top 10 plant pathogenic bacteria in molecular plant pathology. *Mol Plant Pathol* **13**, 614-29 (2012).

19. Preston, G.M. *Pseudomonas syringae* pv. tomato: the right pathogen, of the right plant, at the right time. *Mol Plant Pathol* **1**, 263-75 (2000).

20. Fan et al. High-throughput quantitative luminescence assay of the growth *in planta* of *Pseudomonas syringae* chromosomal tagged with Photorhabdus luminescent luxCDABE. *Plant Journal* **53**(2):393-9 (2008).

21. Meighen, E.A. Molecular biology of bacterial bioluminescence. *Microbiol Rev* **55**, 123-42 (1991).

22. Xin, X.F., Kvitko, B. & He, S.Y. *Pseudomonas syringae*: what it takes to be a pathogen. *Nat Rev Microbiol* **16**, 316-328 (2018).

23. Bender, C.L., Alarcon-Chaidez, F. & Gross, D.C. *Pseudomonas syringae* phytotoxins: mode of action, regulation, and biosynthesis by peptide and polyketide synthetases. Microbiol *Mol Biol Rev* **63**, 266-92 (1999).

24. Bender, C. L., and Scholz-Schroeder, B. K. New insights into the biosynthesis, mode of action, and regulation of syringomycin, syringo- peptin and coronatine. The Pseudomonads. 125-158, ed. *Kluwer Academic Press*, Dordrecht (2004).

25. Jin, Q., Thilmony, R., Zwiesler-Vollick, J. & He, S.Y. Type III protein secretion in *Pseudomonas syringae*. *Microbes Infect* **5**, 301-10 (2003).

26. Brooks, D.M. et al. Identification and characterization of a well-defined series of coronatine biosynthetic mutants of *Pseudomonas syringae* pv. *tomato* DC3000. Mol Plant *Microbe Interact* **17**, 162-74 (2004).

27. Sreedharan, A., Penaloza-Vazquez, A., Kunkel, B.N. & Bender, C.L. CorR regulates multiple components of virulence in *Pseudomonas syringae* pv. *tomato* DC3000. Mol Plant *Microbe Interact* **19**, 768-79 (2006).

28. Fouts, D.E. et al. Genomewide identification of *Pseudomonas syringae* pv. tomato DC3000 promoters controlled by the HrpL alternative sigma factor. *Proc Natl Acad Sci U S A* **99**, 2275-80 (2002).

29. Melotto, M., Underwood, W. & He, S.Y. Role of stomata in plant innate immunity and foliar bacterial diseases. *Annu Rev Phytopathol* **46**, 101-22 (2008).

30. Melotto, M., Underwood, W., Koczan, J., Nomura, K. & He, S.Y. Plant stomata function in innate immunity against bacterial invasion. *Cell* **126**, 969-80 (2006).

31. Navarro, L., Jay, F., Nomura, K., He, S.Y. & Voinnet, O. Suppression of the microRNA pathway by bacterial effector proteins. *Science* **321**, 964-7 (2008).

32. Shivaprasad, P.V. et al. A microRNA superfamily regulates nucleotide binding site-leucine-rich repeats and other mRNAs. *Plant Cell* **24**, 859-74 (2012).

33. Xin, X.F. *et al.* Bacteria establish an aqueous living space in plants crucial for virulence.

Nature **539**, 524-529 (2016).

34. Yu, A. *et al.* Dynamics and biological relevance of DNA demethylation in Arabidopsis

antibacterial defense. *Proc Natl Acad Sci U S A* **110**, 2389-94 (2013).

35. Misas-Villamil, J.C., Kolodziejek, I. & van der Hoorn, R.A. *Pseudomonas syringae* colonizes distant tissues in Nicotiana benthamiana through xylem vessels. *Plant J* **67**, 774-82 (2011).

36. Winston, W.M., Sutherlin, M., Wright, A.J., Feinberg, E.H. & Hunter, C.P. *Caenorhabditis elegans* SID-2 is required for environmental RNA interference. *Proc Natl Acad Sci U S A* **104**, 10565-70 (2007).

37. Whangbo, J.S. & Hunter, C.P. Environmental RNA interference. *Trends Genet* **24**, 297-305 (2008).

38. McEwan, D.L., Weisman, A.S. & Hunter, C.P. Uptake of extracellular double-stranded RNA by SID-2. *Mol Cell* **47**, 746-54 (2012).

39. Feinberg, E.H. & Hunter, C.P. Transport of dsRNA into cells by the transmembrane protein SID-1. *Science* **301**, 1545-7 (2003).

40. Ivashuta, S. et al. Environmental RNAi in herbivorous insects. *RNA* **21**, 840-50 (2015).

41. Daxinger, L. *et al.* Unexpected silencing effects from T-DNA tags in Arabidopsis. *Trends Plant Sci* **13**, 4-6 (2008).

42. Mlotshwa, S. *et al.* Transcriptional silencing induced by Arabidopsis T-DNA mutants is associated with 35S promoter siRNAs and requires genes involved in siRNA-mediated chromatin silencing. *Plant J* **64**, 699-704 (2010).

43. Baldrich, P. et al. Plant Extracellular Vesicles Contain Diverse Small RNA Species and Are Enriched in 10 to 17 Nucleotide "Tiny" RNAs. *Plant Cell* (2019).

44. Rutter, B.D. & Innes, R.W. Extracellular Vesicles Isolated from the Leaf Apoplast Carry Stress-Response Proteins. *Plant Physiol* **173**, 728-741 (2017).

45. Teng, Y. et al. Plant-Derived Exosomal MicroRNAs Shape the Gut Microbiota. *Cell Host Microbe* **24**, 637-652 e8 (2018).

46. Bolognesi, R. et al. Characterizing the mechanism of action of double-stranded RNA activity against western corn rootworm (*Diabrotica virgifera virgifera* LeConte). *PLoS One* **7**, e47534 (2012).

47. Lampropoulos, A. et al. GreenGate - a novel, versatile, and efficient cloning system for plant transgenesis. *PLoS One* **8**, e83043 (2013).

48. Clough, S.J. & Bent, A.F. Floral dip: a simplified method for Agrobacterium-mediated transformation of *Arabidopsis thaliana*. *Plant J* **16**, 735-43 (1998).

49. Castillo-Lizardo, M.G. et al. Contribution of the non-effector members of the HrpL regulon, iaaL and matE, to the virulence of *Pseudomonas syringae* pv. tomato DC3000 in tomato plants. *BMC Microbiol* **15**, 165 (2015).

50. Ross, A. & Somssich, I.E. A DNA-based real-time PCR assay for robust growth quantification of the bacterial pathogen *Pseudomonas syringae* on *Arabidopsis thaliana*. *Plant Methods* **12**, 48 (2016).

51. Kowal, J. *et al.* Proteomic comparison defines novel markers to characterize heterogeneous populations of extracellular vesicle subtypes. *Proc Natl Acad Sci U S A* **113**, E968-77 (2016).

52. Axtell, M.J. ShortStack: comprehensive annotation and quantification of small RNA genes. *RNA* **19**, 740-51 (2013).

53. Lawrence, M. *et al.* Software for computing and annotating genomic ranges. *PLoS Comput Biol* **9**, e1003118 (2013).

54. Li, H. A statistical framework for SNP calling, mutation discovery, association mapping and population genetical parameter estimation from sequencing data. *Bioinformatics* **27**, 2987-93 (2011).

55. Altschul, S.F. *et al.* Gapped BLAST and PSI-BLAST: a new generation of protein database search programs. *Nucleic Acids Res* **25**, 3389-402 (1997).

56. Lorenz, W.A. & Clote, P. Computing the partition function for kinetically trapped RNA secondary structures. *PLoS One* **6**, e16178 (2011).

Acknowledgments

We thank S.-H. He for the *Pto* DC3118-GFP strain, C. Ramos for the *Pto* DC3000 *hrpL* mutant strain, Lorena Martin-Jaular and Federico Cocozza from C. Théry Lab to provide help for the use of the particle tracker analyzer and members of the Navarro laboratory for critical reading of the manuscript. M. S-R., V.M. and L.N. received support by a European Research Council (ERC) “Silencing & Immunity” granted to L.N. (281749). M S-R received additional

Ph.D. funding support under the program “Investissements d'Avenir” and implemented by ANR (ANR-10-LABX-54 MEMO LIFE, ANR-10-IDEX-0001-02PSL). O.T. and A.E.F. received support from the programmes “Jeune Entreprise Innovante” (JEI) and “Crédit Impôt Recherche” (CIR).

Author contributions

M. S-R., M.C., O.T. and A.R. performed the experiments, A.E.F. and V.M. generated some constructs, A.P-Q conducted bioinformatic analyses, M. S-R., O.T., and L.N. analyzed the data; M. S-R., O.T. and L.N. designed the experiments, M. S-R. and L.N. wrote the manuscript, L.N. conceived the overall study.

Competing interests

Two patents have been applied for (PCT/EP2019/072169, PCT/EP2019/072170) on the AGS technology on which M. S-R and L.N. are listed as inventors.

Figure legends

Fig. 1. Stable expression of the IR-*LUXA/LUXB* inverted repeat transgene in Arabidopsis triggers silencing of *Pto* DC3000 *luxA* and *luxB* genes during infection, which is accompanied by a decrease in luminescence activity

a. Schematic representation of the *luxCDABE* operon chromosomally integrated in the genome of *Pto* DC3000[20]. The 250 bp regions of *luxA* (1-250 nt; highlighted region in pink) and *luxB* (1-250 nt; highlighted region in violet) were used to generate the chimeric hairpin construct under the control of the constitutive 35S promoter, hereby designated as $35S_{pro}$:IR-*LUXA/LUXB*. **b.** Accumulation levels of anti-*luxA* and anti-*luxB* siRNAs in the two independent Arabidopsis transgenic lines expressing $35S_{pro}$:IR-*LUXA/LUXB* were detected by low molecular weight northern blot analysis. U6 was used as a loading control. **c.** Luminescence activity of *lux*-tagged *Pto* DC3000 (*Pto* WT LUC) is decreased in the infected Arabidopsis transgenic lines carrying the $35S_{pro}$:IR-*LUXA/LUXB* transgene compared to the infected Col-0 plants. Col-0 plants and IR-*LUXA/LUXB #18* and *#20* transgenic lines were syringe-infiltrated with *Pto* WT LUC at 10^6 cfu ml^{-1}. The bacterial luminescence and titers were monitored at 1 day post-infection (dpi). Four leaves from three plants per condition and from three independent experiments (n) are considered for the analysis. The luminescence activity was estimated by calculating the ratio of bacterial luminescence recorded from individual leaf sample and the number of bacteria (data presented in d.) counted for the corresponding sample. **d.** The IR-*LUXA/LUXB* transgenic lines, *#18* and *#20*, do not exhibit significantly reduced *Pto* WT LUC titer when compared to Col-0-infected plants. Bacterial titers were monitored for the same samples used in c. **e.** Accumulation level of both *luxA* and *luxB* mRNAs are significantly decreased on IR-*LUXA/LUXB*-infected plants compared to Col-0-infected plants. Using the same samples as described in c. and d., bacterial transcript levels of *proC*, *luxA* and *luxB* were monitored by quantitative RT-PCR analysis. These

mRNA levels were quantified relative to the levels of bacterial *gyrA* transcript. Error bars indicate the standard deviations of mRNA values obtained in three independent experiments. Statistically significant differences were assessed using ANOVA test (ns: p-value>0.05; *: p-value<0.05, **: p-value<0.01, ****: p-value<0.0001).

Fig. 2. Stable expression of the IR-*CFA6/HRPL* inverted repeat transgene in Arabidopsis triggers silencing of *Pto* DC3000 *cfa6* and *hrpL* genes during infection

a. Schematic representation of the *Pto* DC3000 genes *cfa6* (in blue) and *hrpL* (in green). The 250 bp regions of *cfa6* (1-250 nt) and *hrpL* (99-348 nt) were used to generate the chimeric hairpin construct under the control of the constitutive 35S promoter. **b.** Representative pictures of five-week old Arabidopsis Col-0 plants and of independent homozygous transgenic plants expressing the $35S_{pro}$:IR-*CYP51* (Control vector: CV) or the $35S_{pro}$:IR-*CFA6/HRPL* transgenes. **c.** Accumulation level of anti-*cfa6* and anti-*hrpL* siRNAs for the Arabidopsis plants depicted in b. was detected by low molecular weight northern blot analysis. U6 was used as a loading control. **d.** Size distribution and abundance of 20-24 nt long sRNA reads from IR-*CFA6/HRPL#4* transgenic line that were mapped to the *cfa6* (upper panel) and *hrpL* (lower panel) regions of the IR-*CFA6/HRPL* sequence. Data from two biological replicates (rep1 and rep2) are presented. **e.** The coverage of sRNA reads which is computed as total count of mapped reads across the IR-*CFA6*/*HRPL* inverted repeat is depicted and include both the plus and minus strand of the construct. **f.** *Pto* DC3000 *hrpL* mRNA accumulation is significantly decreased in the three independent IR-*CFA6/HRPL*-infected transgenic plants compared to Col-0- and CV-infected plants. Arabidopsis plants depicted in b. were dip-inoculated with 10^8 cfu ml^{-1} *Pto* DC3000 WT strain and at 3 days post-infection (dpi), bacterial transcript levels of *proC*, *cfa6* and *hrpL* were monitored by quantitative RT-PCR analysis. These mRNA levels are quantified relative to the level of

bacterial *gyrA* transcripts. Error bars indicate the standard deviations of mRNA values obtained in three independent experiments. Statistically significant differences were assessed using ANOVA test (ns: p-value>0.05; *: p-value<0.05, **: p-value<0.01, ***: p-value<0.001).

Fig. 3. Stable expression of the IR-*CFA6/HRPL* inverted repeat transgene in Arabidopsis suppresses *Pto* DC3000-induced stomatal reopening

a. The *PtoΔcfa6* and *PtoΔhrpL* strains, but not the *PtoΔhrcC* strain, were impaired in their ability to reopen stomata and these phenotypes were rescued upon addition of exogenous COR. Sections of unpeeled leaves of Col-0 plants were incubated with mock solution (water) or 10^8 cfu ml^{-1} of *Pto* DC3000 WT, *Δcfa6*, *ΔhrpL* or *ΔhrcC* strains for 3 hours. Stomatal aperture was assessed by computing the ratio width over length using ImageJ software. **b.** *Pto* DC3000 WT no longer induced stomatal reopening in Arabidopsis transgenic lines overexpressing the IR-*CFA6*/*HRPL* inverted repeat transgene. Stomatal aperture measurement was conducted in Col-0 and IR-*CFA6/HRPL#4*, *#5*, *#10* transgenic lines infected with *Pto* WT strain as described in a. **c.** The *Pto* DC3000-induced stomatal reopening response was unaltered in CV compared to Col-0 plants. Stomatal aperture measurement was conducted in Col-0 and CV plants incubated with *Pto* WT strain as described in a. For all these experiments, n = number of stomata analyzed per condition and statistical significance was assessed using the ANOVA test (ns: p-value > 0.05; ****: p-value < 0.0001). Similar results were obtained from at least three independent experiments (two other biological replicates are presented in Supplementary Fig.3). Pictures at the bottom of the graph depict the representative stomatal aperture phenotypes corresponding to the mean value for each condition/genotype.

Fig. 4. Stable expression of the IR-*CFA6/HRPL* inverted repeat transgene in Arabidopsis inhibits the ability of *Pto* DC3000 to multiply in the apoplast, to mount water-soaking symptoms and to spread in the leaf vasculature

a. Arabidopsis IR-*CFA6/HRPL* transgenic lines exhibit a significantly reduced *Pto* WT titer when compared to Col-0 and CV-infected plants. Col-0, CV and IR-*CFA6/HRPL#4*, *#5* and *#10* plants were dip-inoculated with *Pto* WT-GFP and Col-0 plants were dip-inoculated with the *PtoΔcfa6*-GFP strain. Bacterial titers were monitored at 2 days post-infection (dpi). Four leaves from three plants per condition and from three independent experiments (n) were considered for the comparative analysis. Statistical significance was assessed using the ANOVA test (ns: p-value>0.05; ****: p-value<0.0001). **b.** IR-*CFA6/HRPL#4*, *#5* and *#10* transgenic plants exhibit reduced water-soaking symptoms in comparison to Col-0 and CV plants. Representative leaf pictures of water-soaking symptoms were taken 1 day after dip-inoculation with *Pto* WT-GFP or *PtoΔcfa6*-GFP strain. **c. & d.** IR-*CFA6/HRPL#4*, *#5* and *#10*-infected plants exhibit reduced vascular spreading of *Pto* WT compared to Col-0- and CV-infected plants. Plants were wound-inoculated in midveins with *Pto* WT-GFP and Col-0 was wound-inoculated with *PtoΔcfa6*-GFP. White circles indicate the site of wound-inoculation in the midvein. To index the spreading of bacteria from the inoculation sites, GFP fluorescence signal was observed under UV light and pictures were taken at 3 dpi. When the bacteria propagated away from any of the three inoculation sites, it was indexed as propagation with 4 corresponding to the highest propagation index. Pictures from three biological replicates were taken into consideration and one representative picture is depicted.

Fig. 5. Exogenously applied total RNA extracts from IR-*CFA6/HRPL* plants reduce *Pto* DC3000 pathogenesis in both Arabidopsis and tomato plants

a. *In vitro* AGS assay showing that total RNA extract from IR-*CFA6/HRPL#4* plants triggers silencing of both *cfa6* and *hrpL* genes. *Pto* WT cells were incubated *in vitro* for 4 and 8 hours with 20 ng μl^{-1} of total RNAs from CV or IR-*CFA6/HRPL#4* plants. Significant reduction of the bacterial transcripts *cfa6* and *hrpL* was observed by RT-qPCR at both timepoints, while accumulation of *proC* and *rpoB* transcripts remained unaffected. *gyrA* was used as an internal control to quantify the accumulation of bacterial transcripts. Error bars indicate the standard deviations of values from three independent experiments. **b.** The ability of *Pto* WT to reopen stomata was altered upon exogenous application of total RNA extracts from IR-*CFA6/HRPL* plants compared to CV plants. Col-0 leaves were treated for 1 hour with water or 20 ng μl^{-1} of total RNAs extracted from CV or IR-*CFA6/HRPL#4* plants and were incubated with Pto WT for 3 hours. Stomatal aperture was measured and analyzed as described in Fig.3a. Two other biological replicates are presented in Supplementary Fig.6a. **c.** Pretreatment with IR-*CFA6/HRPL#4* total RNAs reduced the ability of *Pto* DC3000 to multiply in the apoplast of leaves when compared to pretreatment with CV total RNAs. Col-0 leaves were treated with 20 ng μl^{-1} of total RNAs from CV or IR-*CFA6/HRPL#4* plants for 1 hour, followed by dip-inoculation with *Pto* WT. Bacterial titers were monitored at 2 dpi as in Fig.4a. The number of leaves (n) corresponds to collective values from three independent biological replicates. Statistically significant differences were assessed using ANOVA test (ns: p-value>0.05; **: p-value<0.01; ***: p-value<0.001). **d.** The tomato leaves treated with CV total RNAs displayed more necrotic symptoms as compared to the leaves treated with IR-*CFA6/HRPL#4* total RNAs. The experiment was conducted as in c. but using five-week-old tomato (*Solanum lycopersicum*, cultivar 'Moneymaker') plants. Representative pictures of infected leaves in the two conditions are depicted. **e.** A reduced number of *Pto* WT-GFP foci was observed in tomato leaves treated with total RNA extracts from IR-*CFA6/HRPL#4* vs CV plants. Infected-leaves were observed at 3 dpi under UV light to estimate the number of GFP loci. Left panel:

Dot plot representing the number of GFP loci analyzed using ImageJ software from 3-4 different leaves per condition with at least 4 pictures per leaf. The values used for the analysis are from two different independent experiments. Right panel: Representative picture of the tomato leaves described in d. **f.** *Pto* WT-GFP DNA content is decreased in tomato leaves treated with total RNA extracts from IR-*CFA6/HRPL#4* vs CV plants. The level of bacterial DNA content was analyzed by qPCR using tomato *Ubiquitin* gene as a control. For e and f, student's t-test was performed for the comparative analysis (ns: p-value>0.05; **: p-value<0.01; ***: p-value<0.001; ****: p-value<0.0001). Results of another biological replicate for tomato infection assay are presented in Supplementary Fig.5.

Fig. 6. Anti-*cfa6* and anti-*hrpL* small RNA species, but not corresponding unprocessed *CFA6/HRPL* dsRNA precursors, are the RNA entities responsible for AGS and for the suppression of stomatal reopening

a. Accumulation level of IR-*CFA6/HRPL* transcripts in Col-0, *dcl2-1 dcl3-1 dcl4-2* (*dcl234*), IR-*CFA6/HRPL#4* (*#4*) and IR-*CFA6/HRPL#4* in *dcl234* mutant background (*#4* x *dcl234*) was assessed by RT-qPCR. *Ubiquitin* was used as a control. The mean and standard deviation of three independent experiments are represented here. **b.** Accumulation level of anti-*cfa6* and anti-*hrpL* siRNAs in the same genotypes presented in a. were assessed by low molecular weight northern blot analysis. U6 was used as a loading control. **c.** Total RNA extract from *#4* x *dcl234* plants does not alter the transcript accumulation levels of *cfa6* and *hrpL*. *Pto* WT cells were incubated *in vitro* for 8 hours with 20 ng μl^{-1} of total RNAs extracted from the same genotypes described in a. Accumulation levels of *cfa6* and *hrpL* transcripts was assessed by RT-qPCR analysis using *gyrA* as a control. Error bars indicate the standard deviations of values from three independent experiments. **d.** Accumulation level of anti-*cfa6* and anti-*hrpL* siRNAs in the indicated genotypes along with Col-0 plants incubated with total RNAs derived

from the same genotypes for 1 hour were assessed by low molecular weight northern blot analysis. U6 was used as a loading control. Another biological replicate is presented in Supplementary Fig.6b. **e.** Total RNA extract from *#4* x *dcl234* plants does not suppress *Pto* DC3000-induced stomatal reopening response. Col-0 leaves were treated with water or 20 ng μl^{-1} of total RNA extracts from the same genotypes used in a. and incubated with *Pto* WT for 3 hours. Stomatal aperture was measured and analyzed as described in Fig.3a. Two other biological replicates are presented in Supplementary Fig.6c. **f.** Small RNA species, but not the corresponding long RNA species, from IR-*CFA6/HRPL#4* plants suppress stomatal reopening to the same extent as total RNAs extracted from these plants. The experiment was conducted as in d. but with total, long (> 200 nt) or small (< 200 nt) RNA fractions, which were separated from total RNAs of IR-*CFA6/HRPL#4* plants. Two other biological replicates are presented in Supplementary Fig.7c. **g.** Agarose gel picture of ethidium bromide stained in vitro synthesized (IVS) long and small RNA duplexes. **h.** *In vitro*-synthesized (IVS) sRNAs, but not the corresponding long dsRNAs derived from *CFA6/HRPL* chimeric construct, suppressed stomatal reopening. The experiment was conducted as in d. but with *in vitro* synthesized- (IVS), -long or -small RNA species. Long and small RNAs derived from *CYP51* were used as negative controls. Two other biological replicates are presented in Supplementary Fig.7d. **i.** *In vitro* synthesized (IVS) antibacterial siRNAs significantly alter the transcript accumulation levels of *cfa6* and *hrpL*. Accumulation levels of *cfa6* and *hrpL* transcripts were assessed by RT-qPCR analysis using *gyrA* as a control. Error bars indicate the standard deviations of values from three independent experiments. For all the experiments, statistically significant differences were assessed using ANOVA test (ns: p-value>0.05; *: p-value<0.05, **: p-value<0.01, ****: p-value < 0.0001).

Fig. 7. Anti-*hrpL* siRNAs are causal for the silencing of *Pto* DC3000 *hrpL* gene and for the suppression of stomatal reopening

a. Sequence of WT *hrpL* (99-348 nt) selected to generate the inverted repeat transgene (highlighted in yellow) was aligned with the sequence of mutated *hrpL* (mut *hrpL*) designed to contain as many silent mutations as possible in the siRNA targeted region (highlighted in grey). **b.** Unique reads mapping to *hrpL* gene of *Pto* DC3000 in the two sRNA libraries presented in Fig.2d were used for BLAST analysis. The 500 most abundant anti-*hrpL* siRNA reads produced by IR-*CFA6/HRPL#4* plants were selected and blasted against the WT and mut *hrpL* sequences depicted in a. The free energy of binding for each read paired with its top target (lowest *e-value*) was calculated using RNAup and is presented here. Few siRNA-target pairs were above the blast threshold (e-value <10) when the anti-*hrpL* siRNA reads were blasted against the mut *hrpL* sequence (right panel). Thermodynamic energy analysis of these few siRNA-target interactions revealed a mean free energy of binding that was roughly two times higher than the one obtained for the 500 siRNA-target pairs retrieved with the WT *hrpL* sequence (left panel), supporting an impaired binding of the anti-*hrpL* siRNAs towards the mut *hrpL* sequence. **c.** Schematic representation of the *PtoΔhrpL* strain along with the complementation strains generated upon transformation with the plasmids encoding WT *hrpL* or mut *hrpL*, respectively under the control of the constitutive promoter *NPTII*. **d.** *In vitro* AGS assay showing that the *PtoΔhrpL* WT *hrpL* strain is sensitive to antibacterial RNAs while the *PtoΔhrpL* mut *hrpL* is refractory to these RNA entities. *PtoΔhrpL* WT *hrpL* (left panel) and *PtoΔhrpL* mut *hrpL* (right panel) bacterial strains were incubated with total RNAs extracted from CV or IR-*CFA6/HRPL* #4 plants for 8 hours. Accumulation of WT *hrpL* and mut *hrpL* transcripts was analyzed by RT-qPCR. The mRNA levels were quantified relative to the level of *gyrA* transcripts. Error bars indicate the standard deviations of values from three independent experiments. **e.** Accumulation of anti-*cfa6* and anti-*hrpL* siRNAs was

assessed by low molecular weight northern analysis using total RNA extracts from *N. benthamiana* plants transiently expressing 35S$_{pro}$:IR-*HRPL*, 35S$_{pro}$:IR-*CFA6/HRPL* and from non-transformed *N. benthamiana* leaves. U6 was used as a loading control. **f.** Both the WT *hrpL* and mut *hrpL* constructs fully complemented *PtoΔhrpL* for its ability to reopen stomata and only the *PtoΔhrpL* mut *hrpL* strain is refractory to anti-*hrpL* siRNA action. Col-0 leaves were treated with total RNAs extracted either from *N. benthamiana* alone or from *N. benthamiana* expressing the inverted repeat IR-*HRPL* and stomatal reopening response was assessed upon incubation with *PtoΔhrpL* WT *hrpL* and *PtoΔhrpL* mut *hrpL* bacterial strains. Stomatal reopening response was assessed as described previously. Two other biological replicates are presented in Supplementary Fig.9a. **9b g.** Accumulation of anti-*hrpL* siRNAs was assessed by low molecular weight northern analysis using total RNA extracts from Arabidopsis stable transgenic lines expressing the 35S$_{pro}$:IR-*HRPL* transgene. U6 was used as a loading control. **h.** Col-0 and IR-*HRPL#1* and *#4* leaves were treated with water as Mock or indicated bacterial strains for 3 hours prior to stomata aperture measurements. Stomatal reopening response was assessed as described previously. Another biological replicate is presented in Supplementary Fig.9c. For all the stomata experiments, n = number of stomata analyzed per condition. Statistical significance for all the experiments was assessed using the ANOVA test (ns: p-value>0.05; **: p-value<0.001; ****: p-value<0.0001).

Fig. 8. Apoplastic fluid and apoplastic extracellular vesicles (EVs) from Arabidopsis IR-*CFA6/HRPL* plants trigger suppression of *Pto* DC3000-induced stomatal reopening

a. Apoplastic EVs from the Arabidopsis transgenic lines IR-*CYP51* (CV) and IR-*CFA6/HRPL* #4 (#4) were isolated by collecting the apoplastic fluids (APF) from these plants and subjecting them to ultracentrifugation at 40,000g as previously described[44]. The population of particles from the recovered P40 fractions were analyzed using Nanoparticle Tracking

Analysis (NTA). The number of particles, the size of particles according to their diameter (in nm), and the median size of the particles are depicted for each sample. **b.** Both the APF and the P40 fractions triggered full suppression of stomatal reopening. Stomatal aperture was measured in Col-0 leaves that were incubated for 1 hour with the above APF or P40 fractions before being inoculated with *Pto* WT for 3 hours. Results from another biological replicate are presented in Supplementary Fig.10e, 10f. For the stomata experiment, n = number of stomata analyzed per condition and statistical significance was assessed using the ANOVA test (ns: p-value>0.05; ****: p-value<0.0001).

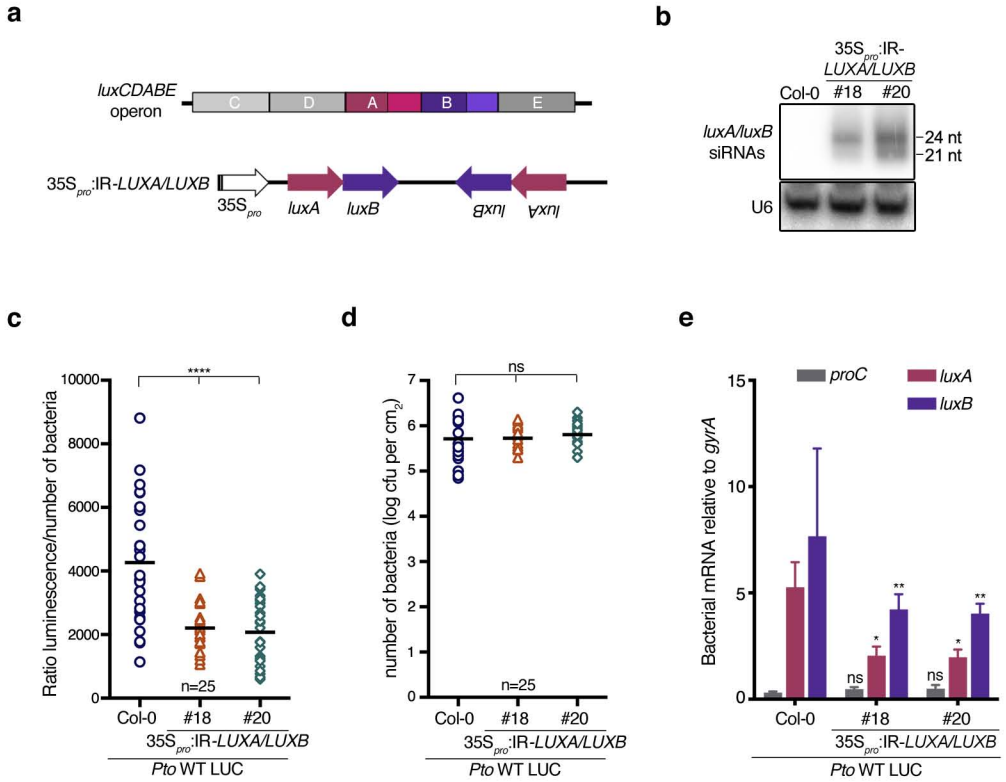

Fig. 1. Stable expression of the IR-*LUXA/LUXB* inverted repeat transgene in Arabidopsis triggers silencing of *Pto* DC3000 *luxA* and *luxB* genes during infection, which is accompanied by a decrease in luminescence activity

a. Schematic representation of the *luxCDABE* operon chromosomally integrated in the genome of inserted in the genome of *Pto* DC3000[20]. The 250 bp regions of *luxA* (1-250 nt; highlighted region in pink) and *luxB* (1-250 nt; highlighted region in violet) were used to generate the chimeric hairpin construct under the control of the constitutive 35S promoter, hereby designated as 35S$_{pro}$:IR-*LUXA/LUXB*. **b.** Accumulation levels of anti-*luxA* and anti-*luxB* siRNAs in the two independent Arabidopsis transgenic lines expressing 35S$_{pro}$:IR-*LUXA/LUXB* were detected by low molecular weight northern blot analysis. U6 was used as a loading control. **c.** Luminescence activity of *lux*-tagged *Pto* DC3000 (*Pto* WT LUC) is decreased in the infected Arabidopsis transgenic lines carrying the 35S$_{pro}$:IR-*LUXA/LUXB* transgene compared to the infected Col-0 plants. Col-0 plants and IR-*LUXA/LUXB #18* and *#20* transgenic lines were syringe-infiltrated with *Pto* WT LUC at 10^6 cfu ml^{-1}. The bacterial luminescence and titers were monitored at 1 day post-infection (dpi). Four leaves from three plants per condition and from three independent experiments (n) are considered for the analysis. The luminescence activity was estimated by calculating the ratio of bacterial luminescence recorded from individual leaf sample and the number of bacteria (data presented in d.) counted for the corresponding sample. **d.** The IR-*LUXA/LUXB* transgenic lines, *#18* and *#20*, do not exhibit significantly reduced *Pto* WT LUC titer when compared to Col-0-infected plants. Bacterial titers were monitored for the same samples used in c. **e.** Accumulation level of both *luxA* and *luxB* mRNAs are significantly decreased on IR-*LUXA/LUXB*-infected plants compared to Col-0-infected plants. Using the same samples as described in c. and d., bacterial transcript levels of *proC*, *luxA* and *luxB* were monitored by quantitative RT-PCR analysis. These mRNA levels were quantified relative to the levels of bacterial *gyrA* transcript. Error bars indicate the standard deviations of mRNA values obtained in three independent experiments. Statistically significant differences were assessed using ANOVA test (ns: p-value>0.05; *: p-value<0.05, **: p-value<0.01, ****: p-value<0.0001).

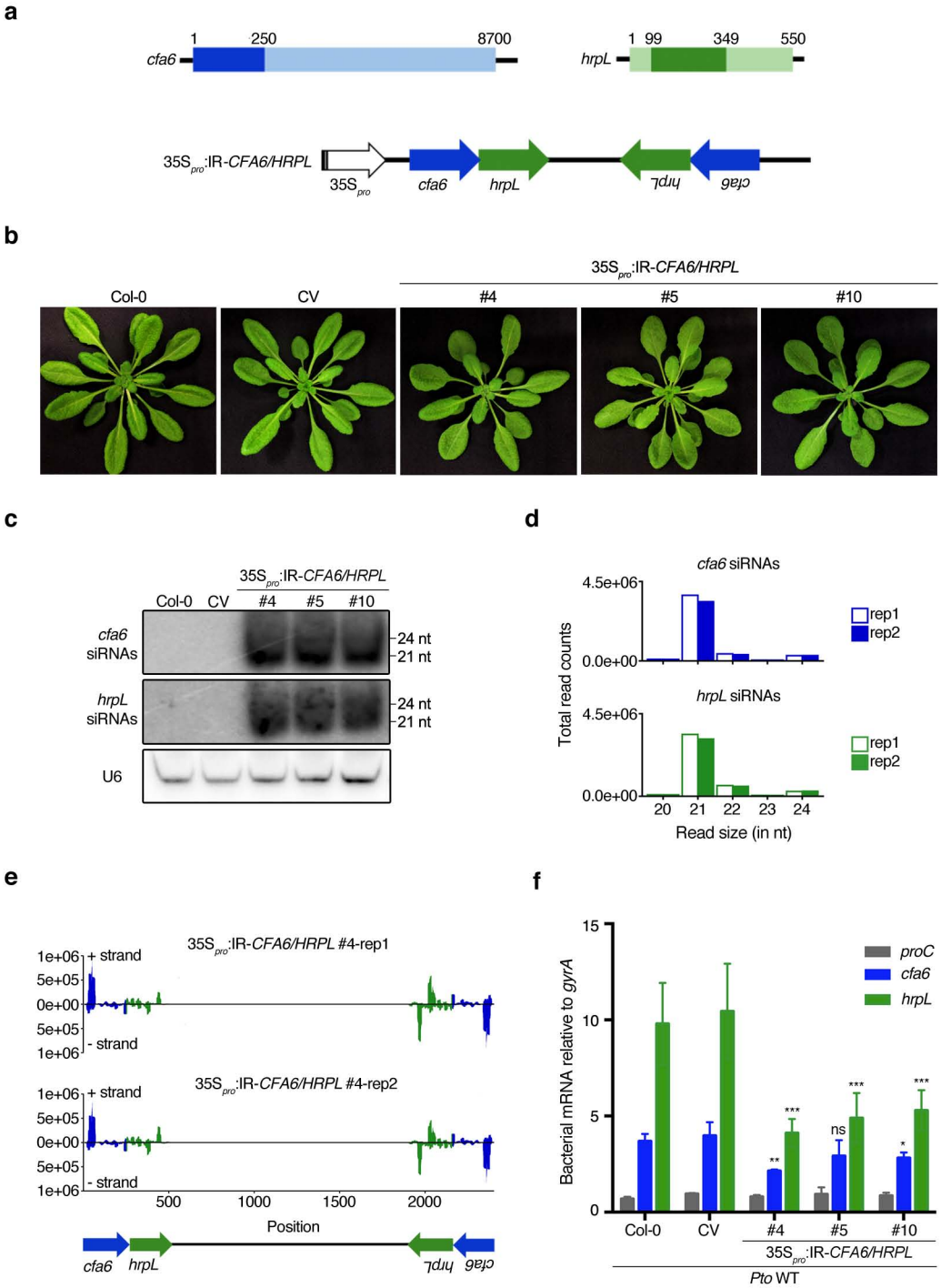

Fig. 2. Stable expression of the IR-*CFA6/HRPL* inverted repeat transgene in Arabidopsis triggers silencing of *Pto* DC3000 *cfa6* and *hrpL* genes during infection
a. Schematic representation of the *Pto* DC3000 genes *cfa6* (in blue) and *hrpL* (in green). The 250 bp regions of *cfa6* (1-250 nt) and *hrpL* (99-348 nt) were used to generate the chimeric hairpin construct under the control of the constitutive 35S promoter. **b.** Representative pictures of five-week old Arabidopsis Col-0 plants and of independent homozygous transgenic plants expressing the $35S_{pro}$:IR-*CYP51* (Control vector: CV) or the $35S_{pro}$:IR-*CFA6/HRPL* transgenes. **c.** Accumulation level of anti-*cfa6* and anti-*hrpL* siRNAs for the Arabidopsis plants depicted in b. were detected by low molecular weight northern blot analysis. U6 was used as a loading control. **d.** Size distribution and abundance of 20-24 nt long sRNA reads form IR-*CFA6/HRPL#4* transgenic line that mapped to the *cfa6* (upper panel) and *hrpL* (lower panel) regions of the IR-*CFA6/HRPL* sequence. Data from two biological replicates (rep1 and rep2) are presented. **e.** The coverage of sRNA reads which is computed as total count of mapped reads across the IR-*CFA6/HRPL* inverted repeat is depicted and include both the plus and minus strand of the construct. **f.** *Pto* DC3000 *hrpL* mRNA accumulation is significantly decreased in the three independent IR-*CFA6/HRPL*-infected transgenic plants compared to Col-0- and CV-infected plants. Arabidopsis plants depicted in b. were dip-inoculated with 10^8 cfu ml^{-1} *Pto* DC3000 WT strain and at 3 days post-infection (dpi), bacterial transcript levels of *proC*, *cfa6* and *hrpL* were monitored by quantitative RT-PCR analysis. These mRNA levels are quantified relative to the level of bacterial *gyrA* transcripts. Error bars indicate the standard deviations of mRNA values obtained in three independent experiments. Statistically significant differences were assessed using ANOVA test (ns: p-value>0.05; *: p-value<0.05, **: p-value<0.01, ***: p-value<0.001).

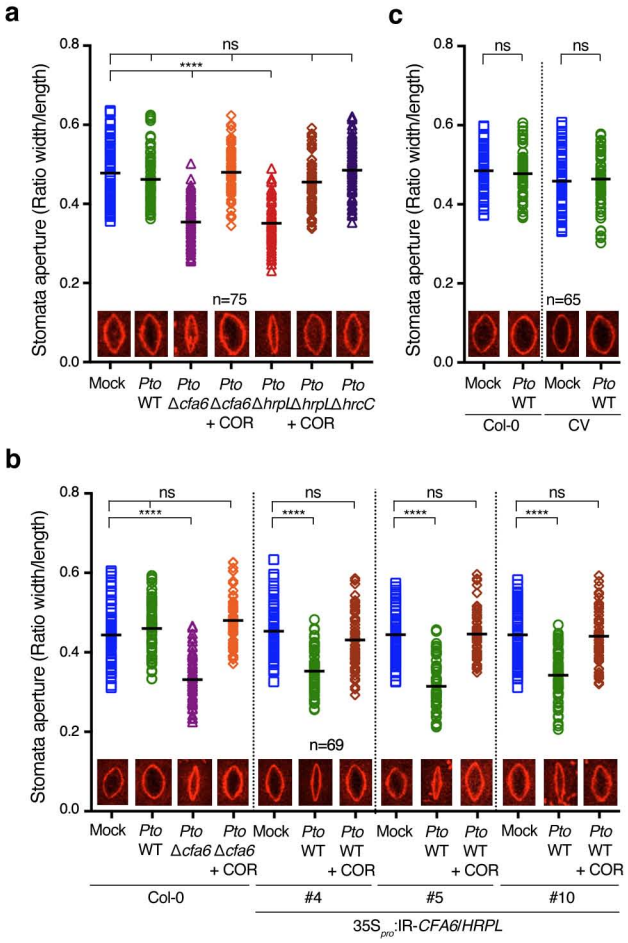

Fig. 3. Stable expression of the IR-*CFA6/HRPL* inverted repeat transgene in Arabidopsis suppresses *Pto* DC3000-induced stomatal reopening

a. The *PtoΔcfa6* and *PtoΔhrpL* strains, but not the *PtoΔhrcC* strain, were impaired in their ability to reopen stomata and these phenotypes were rescued upon addition of exogenous COR. Sections of unpeeled leaves of Col-0 plants were incubated with mock solution (water) or 10^8 cfu ml^{-1} of *Pto* DC3000 WT, *Δcfa6*, *ΔhrpL* or *ΔhrcC* strains for 3 hours. Stomatal aperture was assessed by computing the ratio width over length using ImageJ software. **b.** *Pto* DC3000 WT no longer induced stomatal reopening in Arabidopsis transgenic lines overexpressing the IR-*CFA6/HRPL* inverted repeat transgene. Stomatal aperture measurement was conducted in Col-0 and IR-*CFA6/HRPL #4*, *#5*, *#10* transgenic lines infected with *Pto* WT strain as described in a. **c.** The *Pto* DC3000-induced stomatal reopening response was unaltered in CV compared to Col-0 plants. Stomatal aperture measurement was conducted in Col-0 and CV plants incubated with *Pto* WT strain as described in a. For all these experiments, n = number of stomata analysed per condition and statistical significance was assessed using the ANOVA test (ns: p-value > 0.05; ****: p-value < 0.0001). Similar results were obtained from at least three independent experiments (two other biological replicates are presented in Fig. S3). Pictures at the bottom of the graph depict the representative stomatal aperture phenotypes corresponding to the mean value for each condition/genotype.

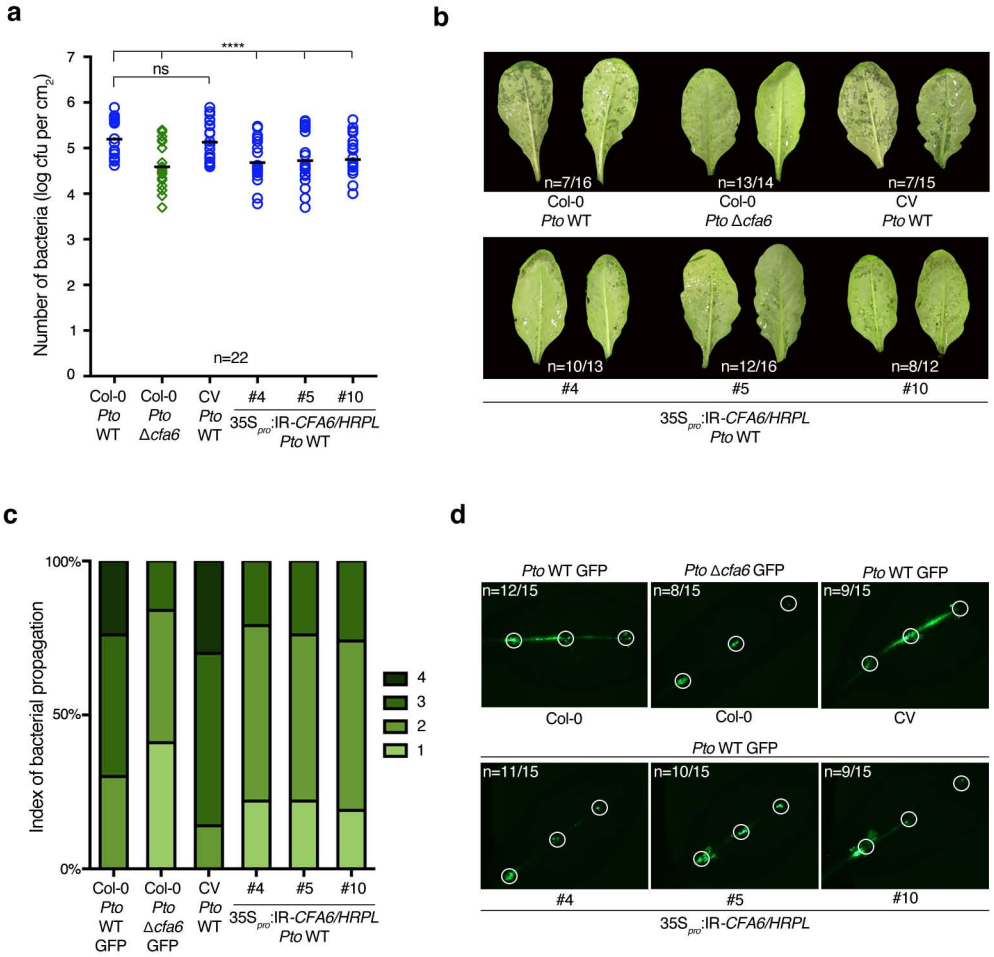

Fig. 4. Stable expression of the IR-*CFA6/HRPL* inverted repeat transgene in Arabidopsis inhibits the ability of *Pto* DC3000 to multiply in the apoplast, to mount water-soaking symptoms and to spread in the leaf vasculature

a. Arabidopsis IR-*CFA6/HRPL* transgenic lines exhibit a significantly reduced *Pto* WT titer when compared to Col-0 and CV-infected plants. Col-0, CV and IR-*CFA6/HRPL#4*, *#5* and *#10* plants were dip-inoculated with *Pto* WT-GFP and Col-0 plants were dip-inoculated with the *PtoΔcfa6*-GFP strain. Bacterial titers were monitored at 2 days post-infection (dpi). Four leaves from three plants per condition and from three independent experiments (n) were considered for the comparative analysis. Statistical significance was assessed using the ANOVA test (ns: p-value>0.05; ****: p-value<0.0001). **b.** IR-*CFA6/HRPL#4*, *#5* and *#10* transgenic plants exhibit reduced water-soaking symptoms in comparison to Col-0 and CV plants. Representative leaf pictures of water-soaking symptoms were taken 1 day after dip-inoculation with *Pto* WT-GFP or *PtoΔcfa6*-GFP strain. **c. & d.** IR-*CFA6/HRPL#4*, *#5* and *#10*-infected plants exhibit reduced vascular spreading of *Pto* WT compared to Col-0- and CV-infected plants. Plants were wound-inoculated in midveins with *Pto* WT-GFP and Col-0 was wound-inoculated with *PtoΔcfa6*-GFP. White circles indicate the site of wound-inoculation in the midvein. To index the spreading of bacteria from the inoculation sites, GFP fluorescence signal was observed under UV light and pictures were taken at 3 dpi. When the bacteria propagated away from any of the three inoculation sites, it was indexed as propagation with 4 corresponding to the highest propagation index. Pictures from three biological replicates were taken into consideration and one representative picture is depicted.

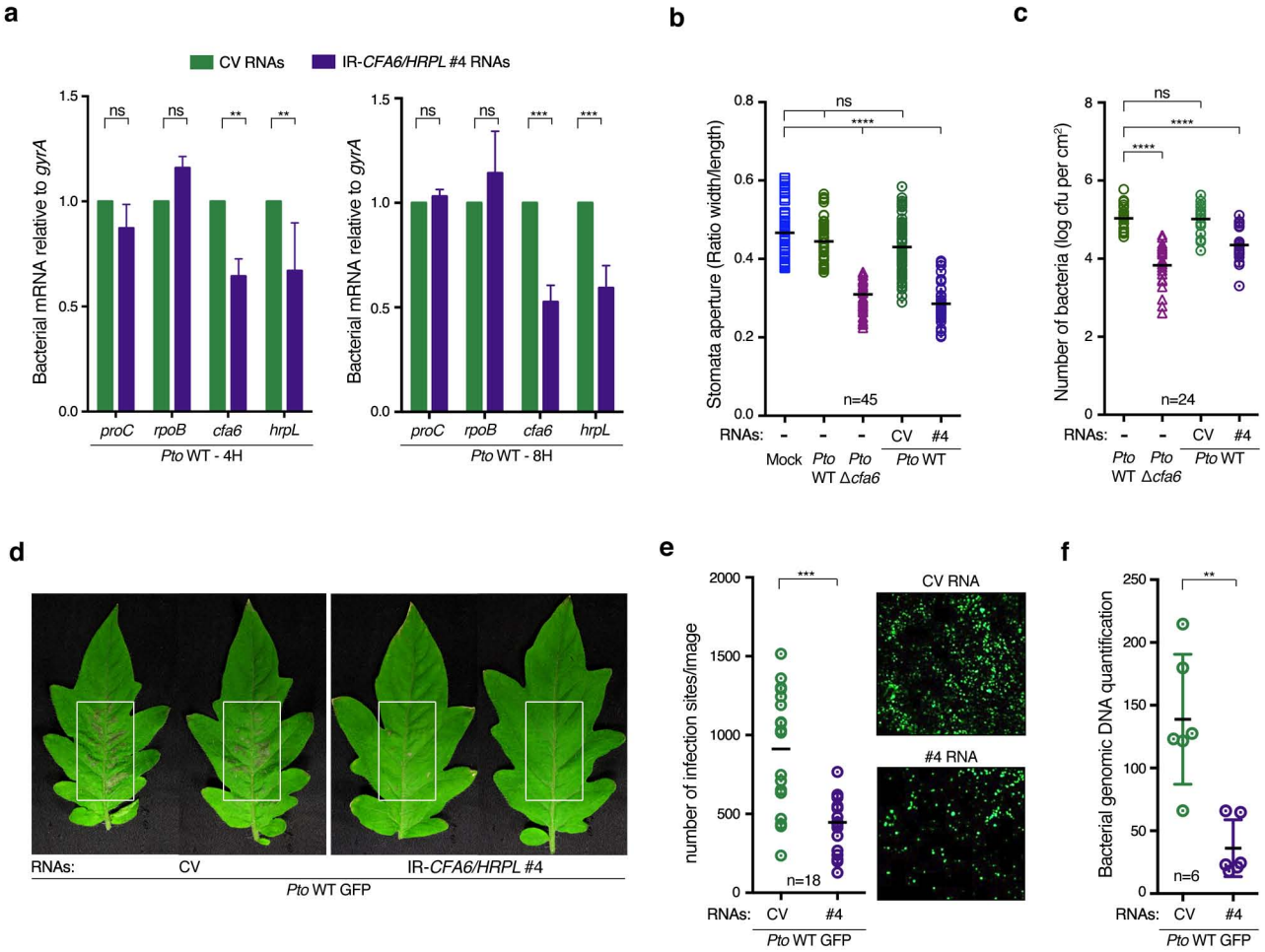

Fig. 5. Exogenously applied total RNA extracts from IR-*CFA6/HRPL* plants reduce *Pto* DC3000 pathogenesis in both Arabidopsis and tomato plants

a. *In vitro* AGS assay showing that total RNA extract from IR-*CFA6/HRPL#4* plants triggers silencing of both *cfa6* and *hrpL* genes. *Pto* WT cells were incubated *in vitro* for 4 and 8 hours with 20 ng µl^{-1} of total RNAs from CV or IR-*CFA6/HRPL#4* plants. Significant reduction of the bacterial transcripts *cfa6* and *hrpL* was observed by RT-qPCR at both the timepoints, while accumulation of *proC* and *rpoB* transcripts remained unaffected. *gyrA* was used as an internal control to quantify the accumulation of bacterial transcripts. Error bars indicate the standard deviations of values from three independent experiments. Statistically significant differences were assessed using ANOVA test (ns: p-value>0.05; **: p-value<0.01, ***: p-value<0.001). **b.** The ability of *Pto* WT to reopen stomata was altered upon exogenous application of total RNA extracts from IR-*CFA6/HRPL* plants compared to CV plants. Col-0 leaves were treated for 1 hour with water or 20 ng µl^{-1} of total RNAs extracted from CV or IR-*CFA6/HRPL#4* plants and were incubated with *Pto* WT for 3 hours. Stomatal aperture was measured and analyzed as described in Fig. 3a. Two other biological replicates are presented in Supplementary Fig. 5a. **c.** Pretreatment with IR-*CFA6/HRPL#4* total RNAs reduced the ability of *Pto* DC3000 to multiply in the apoplast of leaves when compared to pretreatment with CV total RNAs. Col-0 leaves were treated with 20 ng µl^{-1} of total RNAs from CV or IR-*CFA6/HRPL#4* plants for 1 hour, followed by dip-inoculation with *Pto* WT. Bacterial titers were monitored at 2 dpi as in Fig. 4a. The number of leaves (n) corresponds to collective values from three independent biological replicates. **d.** The tomato leaves treated with CV total RNAs displayed more necrotic symptoms as compared to the leaves treated with IR-*CFA6/HRPL#4* total RNAs. The experiment was conducted as in c. but using five-week-old tomato (*Solanum lycopersicum*, cultivar 'Moneymaker') plants. Representative pictures of infected leaves in the two conditions are depicted. **e.** A reduced number of *Pto* WT-GFP foci was observed in tomato leaves treated with total RNA extracts from IR-*CFA6/HRPL#4* vs CV plants. Infected-leaves were observed at 3 dpi under UV light to estimate the number of GFP loci. Left panel: Dot plot representing the number of GFP loci analyzed using ImageJ software from 3-4 different leaves per condition with at least 4 pictures per leaf. The values used for the analysis are from two different independent experiments. Right panel: Representative picture of the tomato leaves described in d. **f.** *Pto* WT-GFP DNA content is decreased in tomato leaves treated with total RNA extracts from IR-*CFA6/HRPL#4* vs CV plants. The level of bacterial DNA content was analyzed by qPCR using tomato *Ubiquitin* gene as a control. For e and f, student's t-test was performed for the comparative analysis (ns: p-value>0.05; **: p-value<0.01; ***:p-value<0.001; ****: p-value<0.0001). Results of another biological replicate for tomato infection assay are presented in Supplementary Fig 5.

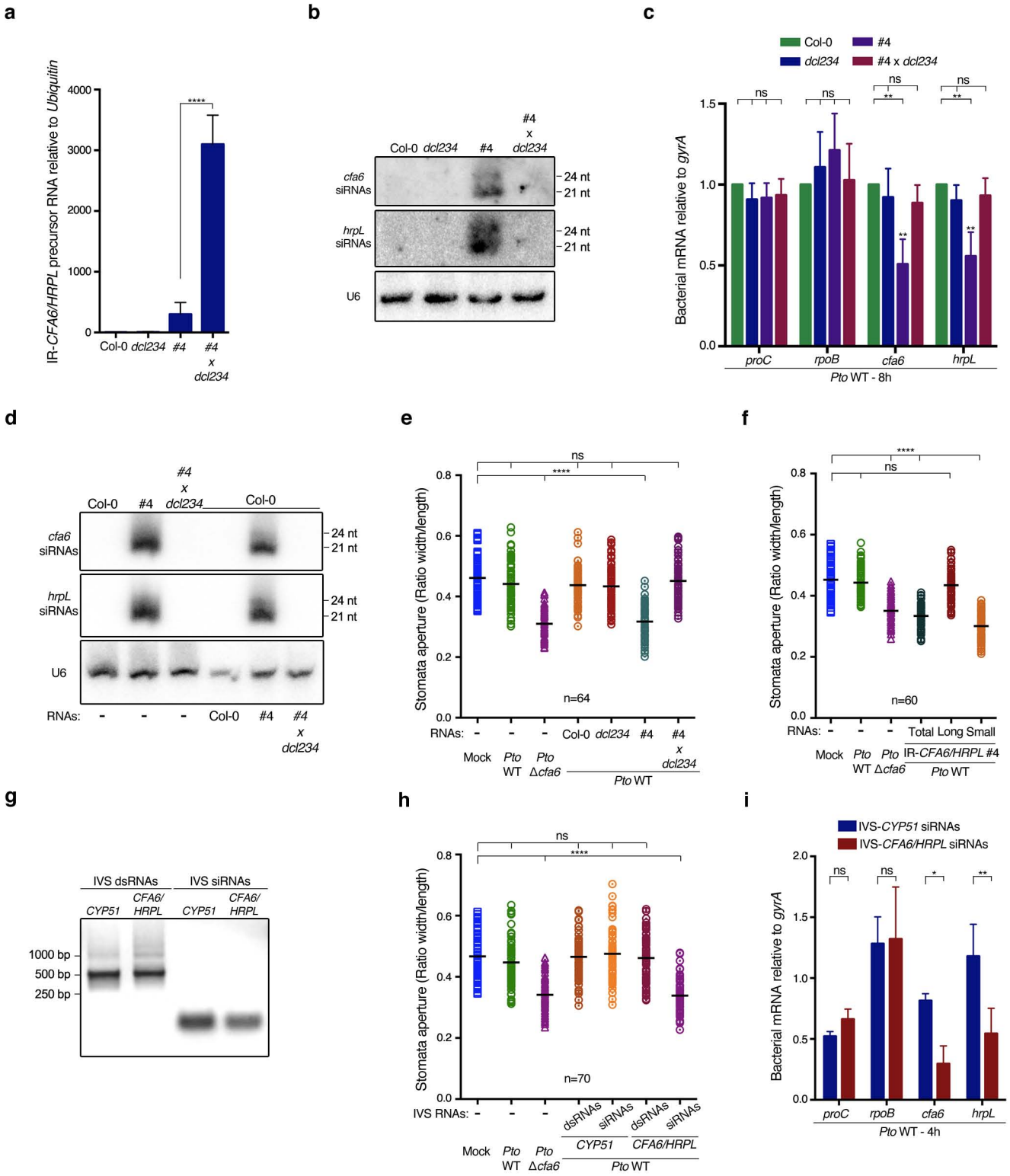

Fig. 6. Anti-*cfa6* and anti-*hrpL* small RNA species, but not corresponding unprocessed *CFA6/HRPL* dsRNA precursors, are the RNA entities responsible for AGS and for the suppression of stomatal reopening

a. Accumulation level of IR-*CFA6/HRPL* transcripts in Col-0, *dcl2-1 dcl3-1 dcl4-2* (*dcl234*), IR-*CFA6/HRPL#4* (*#4*) and IR-*CFA6/HRPL#4* in *dcl234* mutant background (*#4* x *dcl234*) was assessed by RT-qPCR. *Ubiquitin* was used as a control. The mean and standard deviation of three independent experiments are represented here. **b.** Accumulation level of anti-*cfa6* and anti-*hrpL* siRNAs in the same genotypes presented in a. was assessed by low molecular weight northern blot analyses. U6 was used as a loading control. **c.** Total RNA extract from *#4* x *dcl234* plants does not alter the transcript accumulation levels of *cfa6* and *hrpL*. *Pto* WT cells were incubated *in vitro* for 8 hours with 20 ng µl^{-1} of total RNAs extracted from the same genotypes described in a. Accumulation levels of *cfa6* and *hrpL* transcripts was assessed by RT-qPCR analysis using *gyrA* as a control. Error bars indicate the standard deviations of values from three independent experiments. **d .** Accumulation level of anti-*cfa6* and anti-*hrpL* siRNAs in the indicated genotypes along with Col-0 plants incubated with total RNAs derived from the same genotypes for 1 hour was assessed by low molecular weight northern blot analysis. U6 was used as a loading control. Other biological replicate is presented in Supplementary Fig. 6b. **e.** Total RNA extract from *#4* x *dcl234* plants does not suppress *Pto* DC3000-induced stomatal reopening response. Col-0 leaves were treated with water or 20 ng µl^{-1} of total RNA extracts from the same genotypes used in a. and incubated with *Pto* WT for 3 hours. Stomatal aperture was measured and analyzed as described in Fig. 3a. Two other biological replicates are presented in Supplementary Fig. 6c. **f.** Small RNA species, but not the corresponding long RNA species, from IR-*CFA6/HRPL#4* plants suppress stomatal reopening to the same extent as total RNAs extracted from these plants. The experiment was conducted as in d. but with total, long (> 200 nt) or small (< 200 nt) RNA fractions, which were separated from total RNAs of IR-*CFA6/HRPL#4* plants. Two other biological replicates are presented in Supplementary Fig. 7c. **g.** Agarose gel picture of ethidium bromide stained in vitro synthesized (IVS) long and small RNA duplexes. **h.** *In vitro*-synthesized (IVS) sRNAs, but not the corresponding long dsRNAs derived from *CFA6/HRPL* chimeric construct, suppressed stomatal reopening. The experiment was conducted as in d. but with *in vitro* synthesized- (IVS), -long or -small RNA species. Long and small RNAs derived from *CYP51* were used as negative controls. Two other biological replicates are presented in Supplementary Fig. 7e. **i.** *In vitro* synthesized (IVS) antibacterial siRNAs significantly alter the transcript accumulation levels of *cfa6* and *hrpL*. Accumulation level of *cfa6* and *hrpL* transcripts was assessed by RT-qPCR analysis using *gyrA* as a control. Error bars indicate the standard deviations of values from three independent experiments. For all the experiments, statistically significant differences were assessed using ANOVA test (ns: p-value>0.05; *: p-value<0.05, **: p-value<0.01, ****: p-value < 0.0001).

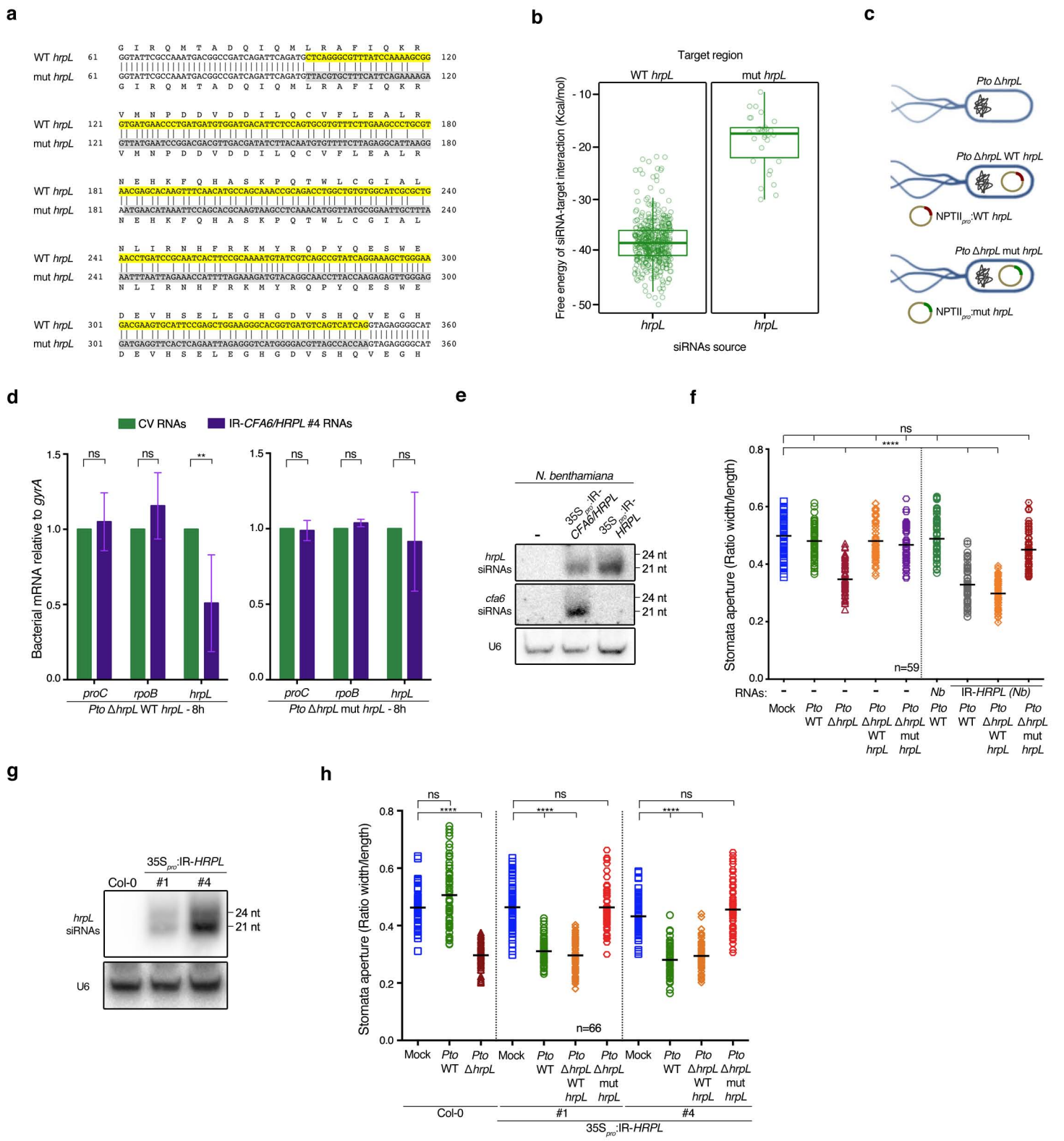

Fig. 7. Anti-*hrpL* siRNAs are causal for the silencing of *Pto* DC3000 *hrpL* gene and for the suppression of stomatal reopening

a. Sequence of WT *hrpL* (99-348 nt) selected to generate the inverted repeat transgene (highlighted in yellow) was aligned with the sequence of mutated *hrpL* (mut *hrpL*) designed to contain as many silent mutations as possible in the siRNA targeted region (highlighted in grey). **b.** Unique reads mapping to *hrpL* gene of *Pto* DC3000 in the two sRNA libraries presented in Fig. 2c were used for BLAST analyses. The 500 most abundant anti-*hrpL* siRNA reads produced by IR-*CFA6/HRPL#4* plants were selected and blasted against the WT *hrpL* and mut *hrpL* sequences depicted in a. The free energy of the top targets with lowest e-values for each read/target pair was calculated using RNAup and is presented here. Few siRNA-target pairs were above the blast threshold when the anti-*hrpL* siRNA reads were blasted against the mut *hrpL* sequence (right panel). Thermodynamic energy analysis of these few siRNA-target interactions revealed a mean free energy that was roughly two times higher than the one obtained for the 500 siRNA-target pairs retrieved with the WT *hrpL* sequence (left panel), supporting an impaired binding of the anti-*hrpL* siRNAs towards the mut *hrpL* sequence. **c.** Schematic representation of the *Pto*Δ*hrpL* strain along with the complementation strains generated upon transformation with the plasmids encoding WT *hrpL* or mut *hrpL*, respectively under the control of the constitutive promoter *NPTII*. **d.** *In vitro* AGS assay showing that the *Pto*Δ*hrpL* WT *hrpL* strain is sensitive to antibacterial RNAs while the *Pto*Δ*hrpL* mut *hrpL* is refractory to these RNA entities. *Pto*Δ*hrpL* WT *hrpL* (left panel) and *Pto*Δ*hrpL* mut *hrpL* (right panel) bacterial strains were incubated with total RNAs extracted from CV or IR-*CFA6/HRPL#4* plants for 8 hours. Accumulation of WT *hrpL* and mut *hrpL* transcripts was analyzed by RT-qPCR. The mRNA levels were quantified relative to the level of *gyrA* transcripts. Error bars indicate the standard deviations of values from three independent experiments. **e.** Accumulation of anti-*cfa6* and anti-*hrpL* siRNAs was assessed by low molecular weight northern analysis using total RNA extracts from *N. benthamiana* plants transiently expressing 35S$_{pro}$:IR-*HRPL*, 35S$_{pro}$:IR-*CFA6/HRPL* and from non-transformed *N. benthamiana* leaves (Nb). U6 was used as a loading control. **f.** Both the WT *hrpL* and mut *hrpL* constructs fully complemented *Pto*Δ*hrpL* for its ability to reopen stomata and only the *Pto*Δ*hrpL* mut *hrpL* strain is refractory to anti-*hrpL* siRNA action. Col-0 leaves were treated with total RNAs extracted either from *N. benthamiana* alone or from *N. benthamiana* expressing the inverted repeat IR-*HRPL* and stomatal reopening response was assessed upon incubating with *Pto*Δ*hrpL* WT *hrpL* and *Pto*Δ*hrpL* mut *hrpL* bacterial strains. Stomatal reopening response was assessed as described previously. Two other biological replicates are presented in Supplementary Fig. 9a. **g.** Accumulation of anti-*hrpL* siRNAs was assessed by low molecular weight northern analysis using total RNA extracts from Arabidopsis stable transgenic lines expressing the 35S$_{pro}$:IR-*HRPL* transgene. U6 was used as a loading control. **h.** Col-0 and IR-*HRPL, #1* and *#4* leaves were treated with water as Mock or indicated bacterial strains for 3 hours prior to stomata aperture measurements. Stomatal reopening response was assessed as described previously. Another biological replicate is presented in Supplementary Fig. 9b. For all the stomata experiments, n = number of stomata analysed per condition. Statistical significance for all the experiments was assessed using the ANOVA test (ns: p-value>0.05; **: p-value<0.001; ****: p-value<0.0001).

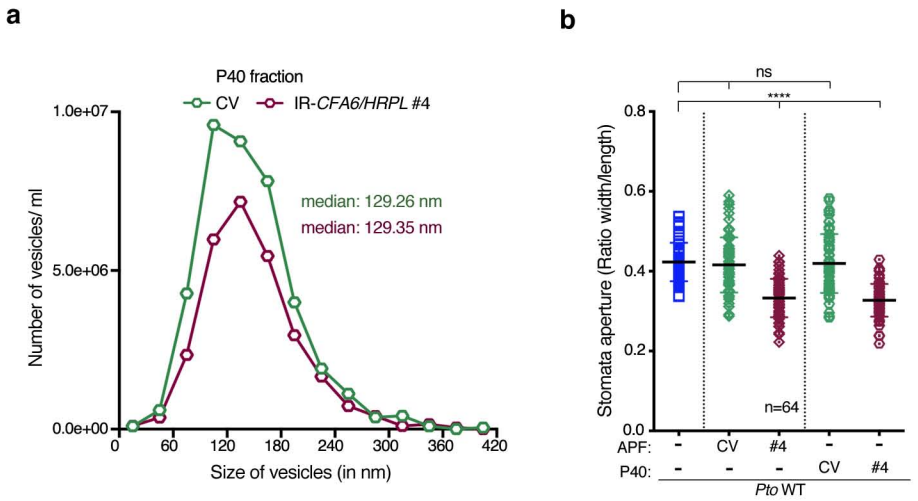

Fig 8. Apoplastic fluid and apoplastic extracellular vesicles (EVs) from Arabidopsis IR-*CFA6/HRPL* plants trigger suppression of *Pto* DC3000-induced stomatal reopening

a. Apoplastic EVs from the Arabidopsis transgenic lines IR-*CYP51* (CV) and IR-*CFA6/HRPL* #4 (#4) were isolated by collecting the apoplastic fluids (APF) from these plants and subjected them to ultracentrifugation at 40,000g as previously described (ref). The population of particles from the recovered P40 fractions were analysed using Nanoparticle Tracking Analysis (NTA). The number of particles, the size of particles according to their diameter (in nm), and the median size of the particles are depicted for each sample. **b.** Both the APF and the P40 fractions triggered full suppression of stomatal reopening. Stomatal aperture was measured in Col-0 leaves that were incubated for 1 hour with the above APF or P40 fractions before being inoculated with *Pto* WT for 3 hours. Results of another biological replicate is presented in Supplementary Fig 10e and 10f. For the stomata experiment, n = number of stomata analysed per condition and statistical significance was assessed using the ANOVA test (ns: p-value>0.05; ****: p-value<0.0001).